

Short-lived Climate Forcers Supplementary Material

Coordinating Lead Authors:

Sophie Szopa (France), Vaishali Naik (United States of America)

Lead Authors:

Bhupesh Adhikary (Nepal), Paulo Artaxo (Brazil), Terje Berntsen (Norway), William D. Collins (United States of America), Sandro Fuzzi (Italy), Laura Gallardo (Chile), Astrid Kiendler-Scharr (Germany/Austria), Zbigniew Klimont (Austria/Poland), Hong Liao (China), Nadine Unger (United Kingdom/United States of America), Prodromos Zanis (Greece)

Contributing Authors:

Wenche Aas (Norway), Dimitris Akritidis (Greece), Robert J. Allen (United States of America), Nicolas Bellouin (United Kingdom/France), Sophie Berger (France/Belgium), Sara M. Blichner (Norway), Josep G. Canadell (Australia), William Collins (United Kingdom), Owen R. Cooper (United States of America), Frank J. Dentener (EU/The Netherlands), Sarah Doherty (United States of America), Jean-Louis Dufresne (France), Sergio Henrique Faria (Spain/Brazil), Piers Forster (United Kingdom), Tzung-May Fu (China), Jan S. Fuglestvedt (Norway), John C. Fyfe (Canada), Aristeidis K. Georgoulias (Greece), Matthew J. Gidden (Austria/ United States of America), Nathan P. Gillett (Canada), Paul Ginoux (United States of America), Paul T. Griffiths (United Kingdom), Jian He (United States of America/China), Christopher Jones (United Kingdom), Svitlana Kravovska (Ukraine), Chaincy Kuo (United States of America), David S. Lee (United Kingdom), Maurice Levasseur (Canada), Martine Lizotte (Canada), Thomas K. Maycock (United States of America), Jean-François Müller (Belgium), Helène Muri (Norway), Lee T. Murray (United States of America), Zebedee R. J. Nicholls (Australia), Jurgita Ovadnevaite (Ireland/Lithuania), Prabir K. Patra (Japan/India), Fabien Paulot (United States of America/France, United States of America), Pallav Purohit (Austria/India), Johannes Quaas (Germany), Joeri Rogelj (United Kingdom/Belgium), Bjørn H. Samset (Norway), Chris Smith (United Kingdom), Izuru Takayabu (Japan), Marianne Tronstad Lund (Norway), Alexandra P. Tsimpidi (Germany/Greece), Steven Turnock United Kingdom), Rita Van Dingene (Italy/Belgium), Hua Zhang (China), Alcide Zhao (United Kingdom/China)

Review Editors:

Yugo Kanaya (Japan), Michael J. Prather (United States of America), Noureddine Yassaa (Algeria)

Chapter Scientist:

Chaincy Kuo (United States of America)

This supplementary material should be cited as:

Szopa, S., V. Naik, B. Adhikary, P. Artaxo, T. Berntsen, W.D. Collins, S. Fuzzi, L. Gallardo, A. Kiendler-Scharr, Z. Klimont, H. Liao, N. Unger, and P. Zanis, 2021: Short-Lived Climate Forcers Supplementary Material. In *Climate Change 2021: The Physical Science Basis. Contribution of Working Group I to the Sixth Assessment Report of the Intergovernmental Panel on Climate Change* [Masson-Delmotte, V., P. Zhai, A. Pirani, S.L. Connors, C. Péan, S. Berger, N. Caud, Y. Chen, L. Goldfarb, M.I. Gomis, M. Huang, K. Leitzell, E. Lonnoy, J.B.R. Matthews, T.K. Maycock, T. Waterfield, O. Yelekçi, R. Yu, and B. Zhou (eds.)]. Available from <https://www.ipcc.ch/>.

Table of Contents

6.SM.1 Methodology for Emissions-based Effective Radiative Forcing	3
6.SM.2 Effective Radiative Forcing and Global Surface Air Temperature Time Series from Emulators for Individual Compounds Over the Historical Period	4
6.SM.3 Regression Coefficient of Annual Mean Surface Ozone and PM_{2.5} Against Annual Surface Temperature Change	5
6.SM.4 Effect on GSAT of a One-year Pulse of Present-day Emissions After 20 and 100 Years	6
6.SM.5 Methodology to Compute Source-Sector Apportionment for Surface Air Pollutants Using TM5-FASST	7
6.SM.6 Data Table	9
References	20

6.SM.1 Methodology for Emissions-based Effective Radiative Forcing

Emissions-based effective radiative forcings (ERFs) are assessed (Figure 6.12, Table 6.SM.1) based on multi-model attribution experiments performed under AerChemMIP (Collins et al., 2017) and analysed by Thornhill et al. (2021). The attribution experiments are done with the precursors' emissions individually perturbed (except carbon monoxide (CO) and non-methane volatile organic compounds (NMVOCs) that were done together). Due to the nonlinear chemistry and microphysics of the atmosphere, the sum of the emissions-based contributions to ERF will not be equal to the concentration-based estimates (Figure 7.6).

The attribution simulations analysed by Thornhill et al. (2021) are for the period 1850–2014, and estimates for the emissions-based ERFs are extrapolated to the full 1750–2019 period based on the updated emissions estimates from the 11 September 2020 version of the Community Emissions Data System (CEDS; Hoesly et al., 2018), obtained from <https://doi.org/10.5281/zenodo.4025316> (see 7.SM.1.3).

For the ozone ERF, in the AerChemMIP experiments the methane concentrations have been kept fixed when the individual precursors are perturbed (e.g., NO_x). This means that methane is not governed by its emissions and the atmospheric chemistry. Thus, adjustments have been made to consider the differences between methane (CH₄) concentrations that would have been reached in a free-to-adjust simulation and a CH₄-fixed simulation. As a consequence of this CH₄ adjustment, a correction has to be applied to all the chemical species which are affected by CH₄ modification, either through chemistry itself (e.g., lifetime) or through stratospheric H₂O changes and cloud changes. Despite these corrections, some nonlinear effects in the chemistry cannot be fully captured and result in differences between

the emissions-based radiative forcing and the concentration-based radiative forcing (Figure 7.6). So finally, only the proportion of the individual effect is kept from this methodology and applied to the concentration-based ERF, which has been determined in a way that allow consideration of all the non-linearities.

The emissions-based ERF estimates for aerosols and aerosol precursors are based on the AerChemMIP simulations (Thornhill et al., 2021). The contribution from aerosol–radiation interactions (ari) is calculated as the difference between the total ERF and the ERF due to aerosol–cloud interactions (ERFaci). Thus, the non-cloud adjustments are included as aerosol–radiation interactions. Because the total aerosol ERFari and ERFaci for 2014 based on AerChemMIP models are more negative and less negative, respectively, compared to that assessed in Chapter 7, the individual aerosol ERFs are scaled relative to total aerosol ERFs in Chapter 7 Section 7.3.3.4 to account for this bias. For black carbon (BC), the cloud effect is assumed to scale with the aerosol ERFari rather than the aerosol ERFaci. For NH₃ emissions ERFaci was not available; the ERF reflects only the aerosol–radiation interactions. As for the ozone precursors, only the proportion of the individual effect is kept from this methodology and applied to the concentration-based ERF.

For CO₂, the fraction of CO₂ in the atmosphere originating from anthropogenic emissions of non-CO₂ emissions (i.e., from CH₄, CO, NMVOCs and halocarbons) must be subtracted from the concentration-based estimate. The sum of carbon emissions via CH₄, halocarbons, NMVOC + CO over the historical period is estimated to be 6.6 GtC, 0.02 GtC and 26 GtC respectively. This includes a rough assumption that 25%, 0%, 50% and 0% of CH₄, halocarbons, NMVOC and CO, respectively, of reactive intermediates such as formaldehyde are lost by deposition. It also assumes that 12% of methane C is still in the atmosphere as methane (Stevenson et al., 2013). Using the CO₂ response function from Joos et al. (2013) to convolve the time profile

Table 6.SM.1 | Effective radiative forcing (ERF, in W m⁻²) by emitted components for the period 1750–2019 as shown in Figure 6.12.

	CO ₂	N ₂ O	CFCs / HCFCs	HFCs	CH ₄	O ₃	H ₂ O (strat)	Aerosol–radiation	Aerosol–cloud	Total ERF	
										Best Estimate	5%–95% range
Components emitted											
CO ₂	2.058									2.058	1.811
CH ₄	0.018				0.844	0.267	0.050	−0.003	0.018	1.195	0.805
N ₂ O		0.210			−0.036	0.026		−0.002	0.043	0.241	0.139
CFC + HCFC + HFC			0.410	0.040	−0.051	−0.162		−0.008	−0.017	0.211	0.020
NO _x					−0.380	0.137		−0.009	−0.014	−0.267	−0.546
NMVOC + CO	0.069				0.162	0.202		−0.003	0.009	0.440	0.215
SO ₂								−0.234	−0.704	−0.938	−1.628
Organic carbon								−0.072	−0.137	−0.209	−0.439
Black carbon								0.145	−0.037	0.107	−0.202
Ammonia								−0.034	0.000	−0.034	−0.042
											−0.026

Table 6.SM.2 | Changes in global mean surface air temperature (GSAT, in °C) due to emitted components for the period 1750–2019 as shown in Figure 6.12.

	CO ₂	N ₂ O	CFCs / HCFCs	HFCs	CH ₄	O ₃	H ₂ O (strat)	Aerosol-radiation	Aerosol-cloud	Total	5–95% range
Components Emitted											
CO ₂	0.951									0.951	0.630
CH ₄	0.009				0.423	0.133	0.025	-0.001	0.007	0.595	0.342
N ₂ O		0.099			-0.017	0.012		-0.001	0.015	0.108	0.054
CFC + HCFC + HFC	0.000		0.194	0.019	-0.024	-0.076		-0.004	-0.006	0.102	0.005
NO _x					-0.197	0.071		-0.005	-0.006	-0.136	-0.298
NMVOC + CO	0.039				0.091	0.114		-0.001	0.004	0.247	0.104
SO ₂								-0.143	-0.324	-0.467	-0.895
Organic carbon								-0.038	-0.055	-0.093	-0.208
Black carbon								0.078	-0.015	0.063	-0.119
Ammonia								-0.016		-0.016	-0.026
											-0.010

of emissions gives a rise in CO₂ of 110 ppb that is proportionally subtracted from the CO₂ total.

For the halogenated compounds, the ERFs for CFCs and HCFCs are taken from Thornhill et al. (2021), and adjusted to include emissions up to 2019. In Figures 6.22 and 6.24 we consider HFCs with lifetimes shorter than about 50 years (as reported by Hodnebrog et al., 2020): HFC-134a, HFC-32, HFC-125, HFC-143a, HFC-152a, HFC-227ea, HFC-245fa, HFC-365mfc, HFC-43-10mee. The ERF from HFCs, taken from the concentration-based estimates (7.SM.1.4) are added, neglecting small effects through changes in OH concentrations affecting HFC lifetime.

6.SM.2 Effective Radiative Forcing and Global Surface Air Temperature Time Series from Emulators for Individual Compounds Over the Historical Period

Global surface air temperature (GSAT) change in response to ERF from short-lived climate forcers (SLCFs) has been estimated using an emulator (see Cross-Chapter Box 7.1 and 7.SM.2) and presented in Figures 6.12, 6.15, 6.22 and 6.24. GSAT changes shown in Figure 6.12 are presented in Table 6.SM.2. The emulator used is an impulse response function (IRF) based on the two-layer energy balance model.

When the ERF time series is known, the response in GSAT at time t is given by:

$$GSAT(t) = \int_{t'=0}^t ERF(t') \times IRF(t-t') dt'$$

Where $t' = 0$ denotes the time when the emission perturbation started, for example, anthropogenic emissions since 1750.

The IRF used here has been calibrated according to the procedure given in 7.SM.2, and is given by:

$$IRF(t) = \sum_{j=1}^J \frac{c_j}{d_j} \exp\left(-\frac{t}{d_j}\right)$$

Where the parameters c_j determine the equilibrium climate response and d_j are time scales of the fast and slow modes of the climate system response, and $J = 2$ here. The parameter values are: $d_1 = 3.4$ years and $d_2 = 285$ years, $c_1 = 0.44 \text{ } ^\circ\text{C } /(\text{W m}^{-2})$ and $c_2 = 0.32 \text{ } ^\circ\text{C } (\text{W m}^{-2})$, corresponding to an ECS of 3.0 $^\circ\text{C}$.

Figure 6.12 shows the historical emissions-based contributions to GSAT (1750–2019). For this analysis the emissions-based ERF time series are based on the AerChemMIP simulations (Thornhill et al., 2021) and are described in 6.SM.1 and 7.SM.1.3. The emissions-based assessment of ERF (6.SM.1) provides ERFs for 2019 relative to 1750, and to establish the ERF time series over the whole historical period, these were scaled back according to the historic emissions (i.e., assuming a linear relation between emissions and ERF historically).

Figure 6.15 shows the GSAT response to step emission reductions of idealized climate forcers with different lifetimes. All forcers are assumed to give an ERF of -1.0 W m^{-2} when a new equilibrium concentration is reached. With this assumption the $ERF(t)$ is given by:

$$ERF(t) = -1.0 \text{ W m}^{-2} \times (1 - e^{-\frac{t}{\tau}})$$

Where τ is the atmospheric lifetime of the climate forcer.

Figures 6.22 and 6.24 show the contributions to GSAT from individual SLCFs, or groups of SLCFs, with an abundance-based perspective. The ERF time series are from the assessment of Chapter 7 of this report and details are given in 7.SM.1.4.

6.SM.3 Regression Coefficient of Annual Mean Surface Ozone and PM_{2.5} Against Annual Surface Temperature Change

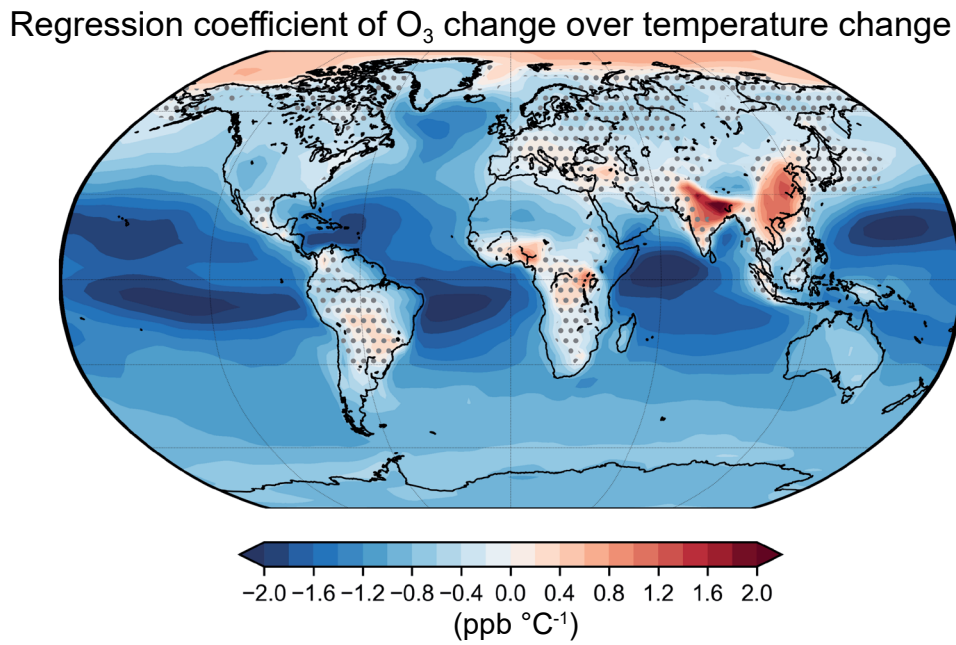


Figure 6.SM.1 | Spatial pattern of the regression coefficient of annual surface ozone change against annual surface temperature change (ppb °C⁻¹) over the 2015 to 2100 period. CMIP6 models include GFDL-ESM4, GISS-E2-1-G, MRI-ESM2-0 and UKESM1-0-LL. For each model, the change in surface O₃ is calculated as the difference between two AerChemMIP experiments – one with evolving future emissions and sea surface temperatures (SSTs) under the SSP3-7.0 scenario (ssp370SST) and the other with the same setup but with fixed present-day SSTs (ssp370pdSST). Regions without dots indicate that modelled regression coefficients are statistically significant (at the 95% significance level) and agree on the sign for at least three out of four models.

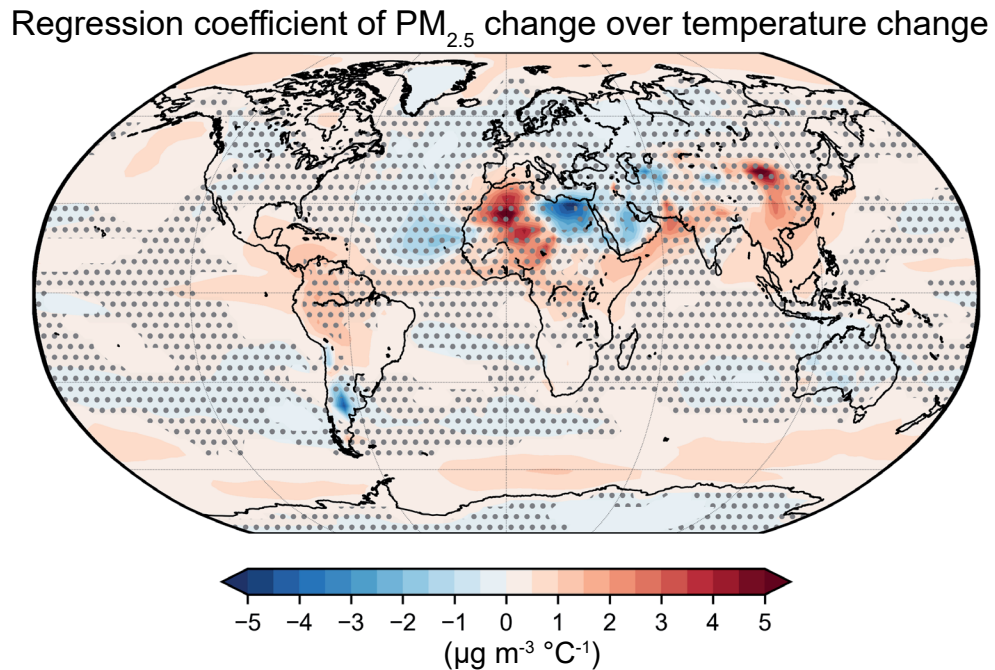


Figure 6.SM.2 | Spatial pattern of the regression coefficient of annual surface PM_{2.5} concentrations change against annual surface temperature change (ppb °C⁻¹) over the 2015 to 2100 period. CMIP6 models include GFDL-ESM4, GISS-E2-1-G, MRI-ESM2-0 and UKESM1-0-LL. For each model, the change in surface PM_{2.5} is calculated as the difference between two AerChemMIP experiments – one with evolving future emissions and sea surface temperatures (SSTs) under the SSP3-7.0 scenario (ssp370SST) and the other with the same setup but with fixed present-day SSTs (ssp370pdSST). Regions without dots indicate that modelled regression coefficients are statistically significant (at the 95% significance level) and agree on the sign for at least two out of three models.

6.SM.4 Effect on GSAT of a One-year Pulse of Present-day Emissions After 20 and 100 Years

The temperature responses in Figure 6.16 and 6.SM.3 were calculated using the concept of absolute global temperature change potential (AGTP; Shine et al., 2005), that is, an emission-metric-based emulator of the climate response to individual emitted species. The approach and further details are documented in Lund et al. (Lund et al., 2020). The emissions were taken from the Community Emissions Data System (CEDS) for the year 2014 (Hoesly et al., 2018), with the exceptions of HFCs, which originate from Purohit et al. (2020) and consider HFCs with a lifetime shorter than 50 years, open biomass burning from van Marle et al. (2017), and aviation water vapour from (Lee et al., 2021). The split between fossil fuel and biofuel emissions in the residential sector, and between the fossil fuel production and distribution and combustion in the energy sector, is based on the GAINS model (ECLIPSE version 6b dataset: https://iiasa.ac.at/web/home/research/researchPrograms/air/Global_emissions.html). CO₂ emissions are excluded from open biomass burning and residential biofuel use due to their unavailability in CEDS and uncertainties around unsustainable emission fraction.

Aviation-specific AGTPs have been calculated for Figure 6.SM.3 using the method described in Lund et al. (Lund et al., 2020) and the best estimate radiative forcing values from Lee et al. (2021). For the HFCs, the AGTPs were derived from Hodnebrog et al. (2020). The AGTPs of BC, SO₂ and OC account for the direct aerosol effect due to aerosol–radiation interactions and are scaled to account for the semi-direct effect of BC due to rapid adjustments and indirect radiative forcing

through aerosol–cloud interactions of sulphate aerosols, respectively. All AGTPs used in the temperature-response calculations now include a carbon–climate feedback term based on the framework by Gasser et al. (2017), except those for HFCs. Avia-contrail refers to the impact from linear contrail formation and subsequent spreading to cirrus clouds, and Avia-stratH₂O to the direct impact of aircraft water vapour emissions.

The error bars show the range (5–95% interval) in the net temperature change due to uncertainty in radiative forcing *only*. This uncertainty range is calculated using a Monte Carlo approach and estimates of uncertainties in global-mean RF of individual species from the literature – see Lund et al. (Lund et al., 2020) for details. The uncertainty in the RF of individual halocarbons was not included due to lack of available data.

The AGTP applies an impulse response function (IRF) to calculate the temperature response as a function of time to a given forcing. The IRF is given by:

$$IRF(t) = \sum_{j=1}^J \frac{c_j}{d_j} \exp\left(-\frac{t}{d_j}\right)$$

where c_j and d_j are constants and time scales of the fast and slow model of the climate system response, respectively, and $j = 2$ here. The IRF used in Lund et al. (Lund et al., 2020) is based on Geoffroy et al. (2013), which yields $d_1 = 4.1$ years and $d_2 = 249$ years, $c_1 = 0.519 \text{ } ^\circ\text{C}/(\text{W m}^{-2})$ and $c_2 = 0.365 \text{ } ^\circ\text{C}/(\text{W m}^{-2})$, corresponding to an ECS of 3.5°C. Note that the IRF used for calculations of GSAT for Figures 6.12, 6.15, 6.22 and 6.24 use an IRF calibrated to the

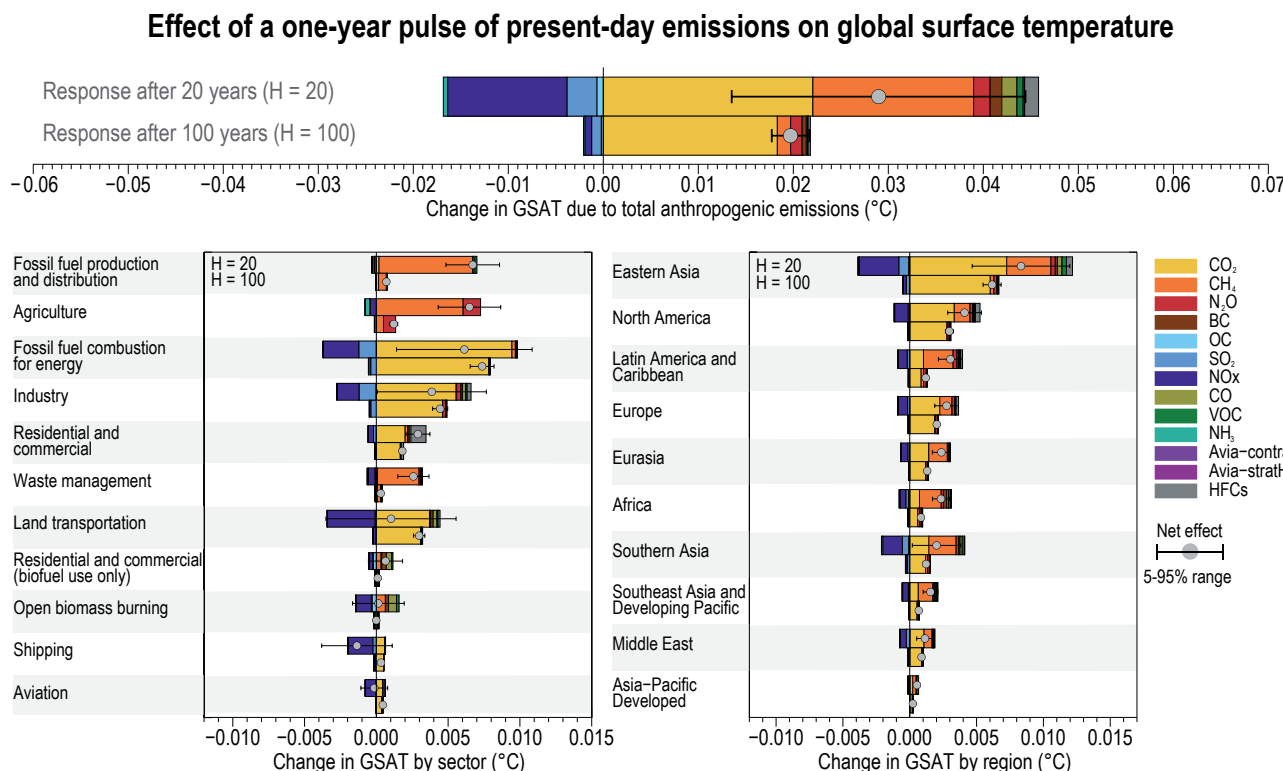


Figure 6.SM.3 | Global mean temperature response 20 and 100 years following one year of present-day (year 2014) emissions.

assessment of ECS and TCR as given in Chapter 7 of this report, and thus use slightly different values for the c_j and d_j constants (see 6.SM.2).

6.SM.5 Methodology to Compute Source-Sector Apportionment for Surface Air Pollutants Using TM5-FASST

Here we provide description of the methodology used to calculate the source-sector apportionment for PM_{2.5} and ozone (Figure 6.17). Furthermore, Figures 6.SM.4 and 6.SM.5 show a comparison of TM5-FASST and ESM models' responses to changes in emissions of PM_{2.5} precursors and ozone.

TM5-FASST is a reduced-form source-receptor model, describing the surface level spatial response of a pollutant metric (concentration, exposure, deposition) to changes in precursor emissions. The model is constructed from pre-computed emission-concentration transfer matrices between pollutant source regions and receptor regions. These matrices reflect underlying meteorological and chemical

atmospheric processes for a predefined set of meteorological and emissions data and have the advantage that concentration responses to emissions changes are obtained by a simple matrix multiplication, avoiding expensive numerical computations.

TM5-FASST's source-receptor matrices have been derived with the chemistry-transport model TM5, by applying 20% emissions perturbations on a reference emissions set (RCP year 2000, year 2001 meteorology) for individual precursors and 56 source regions. The total concentration of component (or metric) j in receptor region y , resulting from given emissions E of all n_j precursors i at all n_x source regions x , is obtained as a perturbation on the base-simulation concentration, by summing up all the respective source-receptor coefficients A , scaled with the actual emissions perturbation:

$$C_j(y) = C_{j,\text{ref}}(y) + \sum_{k=1}^{n_x} \sum_{i=1}^{n_j} A_{ij}[x_k, y] \cdot [E_i(x_k) - E_{i,\text{ref}}(x_k)]$$

where $A_{ij}[x_k, y] = \frac{\Delta C_{j,\text{ref}}(y)}{0.2 E_{i,\text{ref}}(x_k)}$, the pre-computed source-receptor coefficient for source region x_k to receptor region y , for precursor i contributing to metric/pollutant j . The computational efficiency from

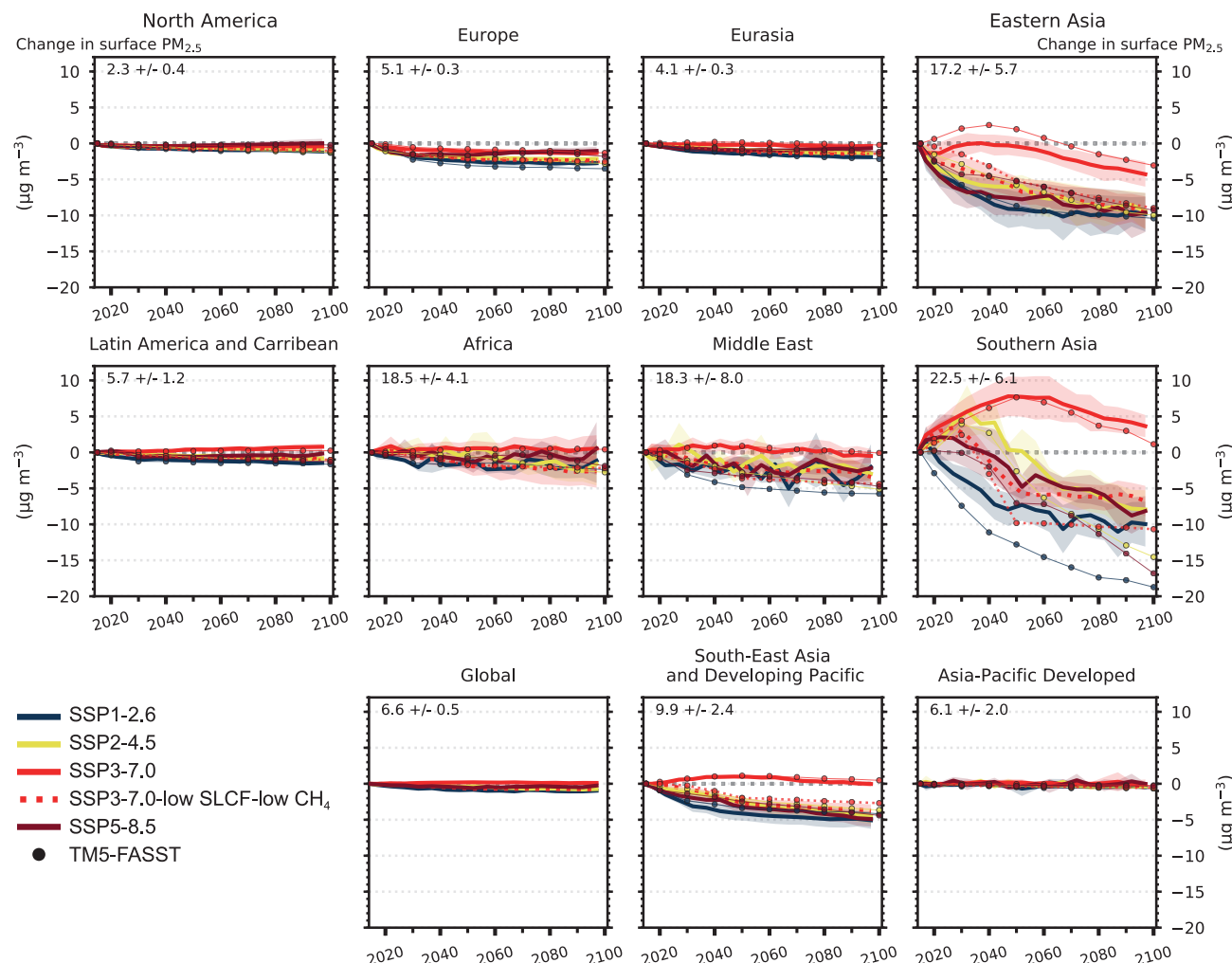


Figure 6.SM.4 | Future global and regional changes in annual mean surface PM_{2.5}, relative to the 2005–2014 mean, for the different SSPs used in CMIP6. Each line represents a multi-model mean across the region with shading representing the ± 1 standard deviation in the mean. Dots represent TM5-FASST results. The multi-model regional mean value (± 1 standard deviation) for the year 2005–2014 is shown in the top-left corner of each panel.

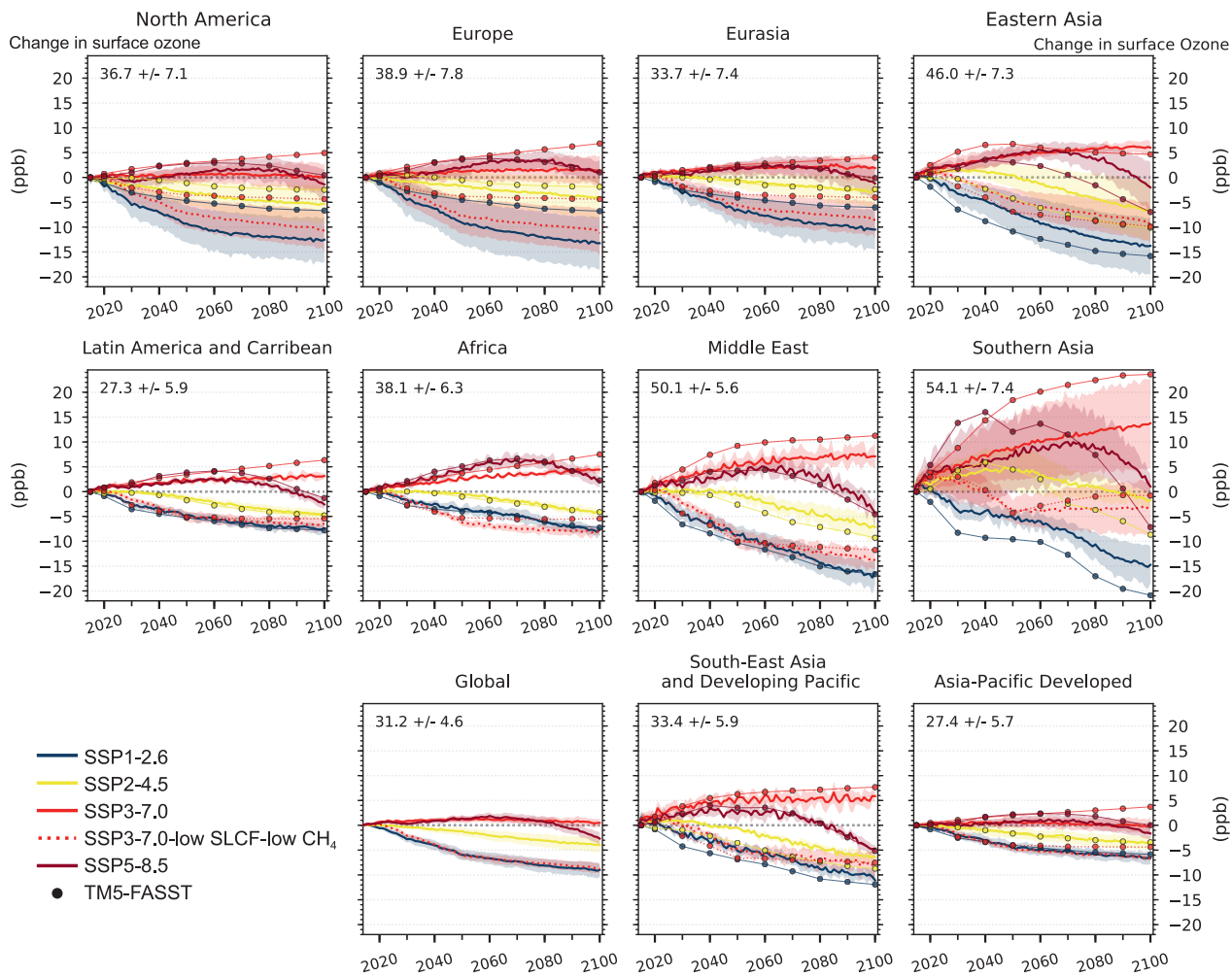


Figure 6.SM.5 | Future global and regional changes in annual mean surface O₃, relative to the 2005–2014 mean, for the different SSPs used in CMIP6.
Each line represents a multi-model mean across the region with shading representing the ± 1 standard deviation around the mean. Dots represent TM5-FASST results. The multi-model regional mean value (± 1 standard deviation) for the year 2005–2014 is shown in the top-left corner of each panel.

the linearized emission-concentration sensitivities comes at some cost of accuracy, in particular because the model bypasses underlying mechanisms describing chemical and meteorological feedback processes that could lead to nonlinear responses.

TM5-FASST computes PM_{2.5} concentrations from precursor emissions of SO₂, NO_x, NH₃, elemental carbon and particulate organic matter. Secondary organic matter from anthropogenic emissions is not included. Ozone concentrations and long-term exposure metrics are computed from NO_x, NMVOC and methane precursor emissions. CO as an ozone precursor is not included. The methane–ozone response is assumed to be instantaneous, neglecting the perturbation lifetime of more than a decade (Section 6.3.1).

The computational efficiency of TM5-FASST allows for multiple runs exploring source attribution by region or emissions source. We estimate the relative contribution of individual emissions sectors shown in Figure 6.17 by subtracting their emissions one by one from the total emissions in Eq. (1) and computing the resulting concentration. Subtracting this result from the total concentration (Eq. 1) yields each sector's contribution (Karagulian et al., 2016).

TM5-FASST has been extensively documented and evaluated by Van Dingenen et al. (2018). The model has been applied in a variety of assessment studies (e.g., Brauer et al., 2016; Rao et al., 2017; Aakre et al., 2018; Markandya et al., 2018; Crippa et al., 2019; Harmsen et al., 2020; Kühn et al., 2020; Rauner et al., 2020; Vandycy et al., 2020). Validation studies in Van Dingenen et al. (2018) show that, despite inherent simplifications and caveats, large-scale PM_{2.5} and O₃ responses to emissions changes in TM5-FASST compare well with the chemical transport model TM5. Figure 6.SM.4 and 6.SM.5 compare TM5-FASST regional PM_{2.5} and O₃ responses to emissions changes with the ensemble of ESM models for selected SSP scenarios. In nearly all cases TM5-FASST results fall within ± 1 standard deviation of the CMIP6 ESM ensemble. Notable differences are observed for the SSP scenarios and regions representing more extreme emissions changes (in particular for the low-emission scenarios in Southern Asia). As documented by Van Dingenen et al. (2018), for both PM_{2.5} and O₃ the differences with full-process models can be attributed to nonlinear responses to NO_x-emission reductions that are not captured by the linearized source-receptor model.

6.SM.6 Data Table

Table 6.SM.3 | Input data table. Input datasets and code used to create chapter figures.

Figure Number	Dataset Name	Type of Dataset	File Name	License Type	Dataset Citation	Dataset DOI/URL	Citation for Relevant Papers	Notes
Figure 6.3	Community Emissions Data System (CEDS)	Input dataset	CMIP6 Data Release (data only) July 26, 2016 for CEDS	Public	Hoesly et al. (2018)	www.globalchange.umd.edu/ceds/ (accessed 28/01/2022) https://github.com/JGCRI/CEDS/ (accessed 28/01/2022)		
Figure 6.4	CMIP6, ScenarioMIP, Tropospheric Ozone Assessment Report (TOAR), Atmospheric Chemistry and Climate Model Intercomparison Project (ACCMIP)	Input dataset	CMIP6 models: UKESM1-LL-0, CESM2-WACCM, GFDL-ESM4, MRI-ESM2-0, GISS-E2.1-G Experiments: historical experiment, SSP3-7.0	https://esgf.llnl.gov/LICENSE.html	Eyring et al. (2016); O'Neill et al. (2016)	https://esgf-node.llnl.gov/search/cmip6/ (accessed 28/01/2022)	Griffiths et al. (2020); Young et al. (2013, 2018)	
	Observational datasets: TOST, IASI-FORLI, IASI-OFRID, OMI/MLS, OMI-SAI, OMI-RAL	Input dataset		Public		https://doi.org/10.1525/elementa.291.t1 (accessed 28/01/2022)	Gaudel et al. (2018)	
CMIP6 data citations								
	CESM2-WACCM: historical, ssp370	Input dataset			Danabasoglu (2019a, b)	https://esgf-node.llnl.gov/search/cmip6/ (accessed 28/01/2022)		
	GFDL-ESM4: esm-hist, historical, ssp370	Input dataset			John et al. (2018c); Krasting et al. (2018a, b)	https://esgf-node.llnl.gov/search/cmip6/ (accessed 28/01/2022)		
	GISS-E2-1-G: historical, ssp370	Input dataset			NASA Goddard Institute for Space Studies (NASA/GISS) (2018, 2020i)	https://esgf-node.llnl.gov/search/cmip6/ (accessed 28/01/2022)		
	MRI-ESM2-0: historical, ssp370	Input dataset			Yukimoto et al. (2019e, j)	https://esgf-node.llnl.gov/search/cmip6/ (accessed 28/01/2022)		
	UKESM1-0-LL: historical, ssp370	Input dataset			Good et al. (2019c); Tang et al. (2019)	https://esgf-node.llnl.gov/search/cmip6/ (accessed 28/01/2022)		
Figure 6.5	IAGOS-CORE	Input dataset	Decadal	Public	Gaudel et al. (2020)	www.iagos-data.fr/portal.html#TimeseriesPlace (accessed 28/01/2022)	Cooper et al. (2020)	
Figure 6.6	Merged GOME/SCIAMACHY/GOME-2 (TM4NO2A version 2.3)	Input dataset	GOME_SCIAMACHY_GOME2ab_TroposNO2_v2.3_041996-092017_temis.nc	Public			Georgoulias et al. (2019)	

Figure Number	Dataset Name	Type of Dataset	File Name	License Type	Dataset Citation	Dataset DOI/URL	Citation for Relevant Papers	Notes
Figure 6.7	EPA PM _{2.5} aerosol component	Input dataset	Monthly average 2000–2018	Public		https://aqs.epa.gov/aqswb/airdata/download_files.html (accessed 28/01/2022)	Solomon et al. (2014)	
	IMPROVE aerosol	Input dataset	Monthly average daily 2000–2018	Public		http://views.cira.colostate.edu/fed/QueryWizard/Default.aspx		
	EMEP PM _{2.5} aerosol component	Input dataset	Monthly average 2000–2018	Public		www.emep.int/ (accessed 28/01/2022)		
	Network Center for EANET, EANET data on acid deposition in the East Asian region, PM _{2.5} aerosol component	Input dataset	Monthly average 2001–2017	Public				
	SPARTAN PM _{2.5} aerosol component	Input dataset	Monthly average 2013–2019	Public		www.spartan-network.org/ (accessed 28/01/2022)	Snider et al. (2015)	
	Observational field campaigns PM _{2.5} aerosol component over Latin America and Caribbean, Africa, Europe, Eastern Asia and Asia-Pacific Developed	Input dataset		Public			Celis et al. (2004); Feng et al. (2006); Bourotte et al. (2007); Fuzzi et al. (2007); Mariani and de Mello, 2007; Molina et al. (2007, 2010); Favez et al. (2008); Mkoma, 2008; Aggarwal and Kawamura, 2009; Mkoma et al. (2009); de Souza et al. (2010); Li et al. (2010); Martin et al. (2010); Radhi et al. (2010); Weinstein et al. (2010); Batmunkh et al. (2011); Gioda et al. (2011); Pathak et al. (2011); Zhang et al. (2012); Cho and Park, 2013; Zhao et al. (2013); Wang et al. (2019); Kuzu et al. (2020)	
		Intermediate dataset				https://github.com/IPCC-WG1/Chapter-6		
Figure 6.8	CMIP6 ambient aerosol optical thickness at 550 nm	Input dataset Annual average	Historical experiment, models: ACCESS-CM2, BCC-ESM1, CESM2-FV2, CESM2-WACCM, CESM2, CNRM-CM6-1, CNRM-EMS2-1, CanESM5, E3SM-1-0, GFDL-CM4, GFDL-ESM4, GISS-E2-1-G, HadGEM3-GC31-LL, INM-CM4-8, IPSL-CM6A-LR, KACE-1-0-G, MIROC-ES2L, MPI-ESM-1-2, MPI-ESM1-2-HR, MPI-ESM1-2-LR, MRI-ESM2-0, NorESM2-LM, UKESM1-0-LL	https://esgf.llnl.gov/LICENSE.html	Eyring et al. (2016); O'Neill et al. (2016)	https://esgf-node.llnl.gov/search/cmip6/ (accessed 28/01/2022)		

Figure Number	Dataset Name	Type of Dataset	File Name	License Type	Dataset Citation	Dataset DOI/URL	Citation for Relevant Papers	Notes
Figure 6.9	CMIP6, mole fraction hydroxyl in air	Input dataset Decadal average	Models: UKESM1-0LL, GFDL-ESM4, CESM2-WACCM	Public	Eyring et al. (2016)	https://esgf-node.llnl.gov/search/cmip6/ (accessed 28/01/2022)	Montzka et al. (2011); Rigby et al. (2017); Turner et al. (2017); Nicely et al. (2018); Naus et al. (2019); Patra et al. (2021)	
	CMIP6 data citations							
	CESM2-WACCM: historical	Input dataset			Danabasoglu (2019a)	https://esgf-node.llnl.gov/search/cmip6/ (accessed 28/01/2022)		
	GFDL-ESM4: historical	Input dataset			Krasting et al. (2018b)	https://esgf-node.llnl.gov/search/cmip6/ (accessed 28/01/2022)		
	UKESM1-0-LL: historical	Input dataset		https://esgf.llnl.gov/LICENSE.html	Tang et al. (2019)	https://esgf-node.llnl.gov/search/cmip6/ (accessed 28/01/2022)		
	CMIP6: AerChemMIP experiments histSST and histSST-piAer. Output variables rsut and rlut.	Input dataset Averaged from monthly output	Models: MIROC6, MPI-ESM-1-2-HAM, GISS-E2-1-G, NorESM2-LM, MRI-ESM2-0, GFDL-ESM4, UKESM-0-LL	Public	Eyring et al. (2016); Collins et al. (2017)	https://esgf-node.llnl.gov/search/cmip6/ (accessed 28/01/2022)		
		Intermediate dataset				https://github.com/IPCC-WG1/Chapter-6		
Figure 6.10	CMIP6 data citations							
	GFDL-ESM4: histSST, histSST-piAer	Input dataset			Horowitz et al. (2018c, d)	https://esgf-node.llnl.gov/search/cmip6/ (accessed 28/01/2022)		
	GISS-E2-1-G: histSST, histSST-piAer	Input dataset			NASA Goddard Institute for Space Studies (NASA/GISS) (2019c, d)	https://esgf-node.llnl.gov/search/cmip6/ (accessed 28/01/2022)		
	MIROC6: histSST, histSST-piAer	Input dataset			Takemura (2019c, d)	https://esgf-node.llnl.gov/search/cmip6/ (accessed 28/01/2022)		
	MPI-ESM-1-2-HAM: histSST, histSST-piAer	Input dataset			Neubauer et al. (2019a, b)	https://esgf-node.llnl.gov/search/cmip6/ (accessed 28/01/2022)		
	MRI-ESM2-0: histSST, histSST-piAer	Input dataset			Yukimoto et al. (2019b, 2020b)	https://esgf-node.llnl.gov/search/cmip6/ (accessed 28/01/2022)		
	NorESM2-LM: histSST, histSST-piAer	Input dataset			Olivie et al. (2019c, d)	https://esgf-node.llnl.gov/search/cmip6/ (accessed 28/01/2022)		
	UKESM1-0-LL: histSST, histSST-piAer	Input dataset			O'Connor (2019c, d)	https://esgf-node.llnl.gov/search/cmip6/ (accessed 28/01/2022)		

Figure Number	Dataset Name	Type of Dataset	File Name	License Type	Dataset Citation	Dataset DOI/URL	Citation for Relevant Papers	Notes
Figure 6.11	CMIP6: AerChemMIP experiments histSST and histSST-piAer. Output variables rsut and rlut	Input dataset Averaged from monthly output	Models: MIROC6, MPI-ESM-1-2-HAM, GISS-E2-1-G, NorESM2-LM, MRI-ESM2-0, GFDL-ESM4, UKESM-0-LL	https://esgf.llnl.gov/LICENSE.html	Eyring et al. (2016); Collins et al. (2017)	https://esgf-node.llnl.gov/search/cmip6/ (accessed 28/01/2022)		
	CMIP6 data citations							
	GFDL-ESM4: histSST, histSST-piAer	Input dataset			Horowitz et al. (2018c, d)	https://esgf-node.llnl.gov/search/cmip6/ (accessed 28/01/2022)		
	GISS-E2-1-G: histSST, histSST-piAer	Input dataset			NASA Goddard Institute for Space Studies (NASA/GISS) (2019c, d)	https://esgf-node.llnl.gov/search/cmip6/ (accessed 28/01/2022)		
	MIROC6: histSST, histSST-piAer	Input dataset			Takemura (2019c, d)	https://esgf-node.llnl.gov/search/cmip6/ (accessed 28/01/2022)		
	MPI-ESM-1-2-HAM: histSST, histSST-piAer	Input dataset			Neubauer et al. (2019a, b)	https://esgf-node.llnl.gov/search/cmip6/ (accessed 28/01/2022)		
	MRI-ESM2-0: histSST, histSST-piAer	Input dataset			Yukimoto et al. (2019b, 2020b)	https://esgf-node.llnl.gov/search/cmip6/ (accessed 28/01/2022)		
	NorESM2-LM: histSST, histSST-piAer	Input dataset			Olivie et al. (2019c, d)	https://esgf-node.llnl.gov/search/cmip6/ (accessed 28/01/2022)		
Figure 6.12	UKESM1-0-LL: histSST, histSST-piAer	Input dataset			O'Connor (2019c, d)	https://esgf-node.llnl.gov/search/cmip6/ (accessed 28/01/2022)		
	Figure 6.12 code	Code					Ghan (2013); Joos et al. (2013); Stevenson et al. (2013); Thornhill et al. (2021)	See IPCC AR6 WGI 6.SM.1, 6.SM.2 for details and 7.SM.1
Figure 6.13	CMIP6: AerChemMIP experiments historical and hist-piAer. Output variable: tas	Intermediate dataset	Models: MIROC6, MRI-ESM2-0, NorESM2-LM, GFDL-ESM4, GISS-E2-1-G, UKESM1-0-LL	https://esgf.llnl.gov/LICENSE.html	Eyring et al. (2016); Collins et al. (2017)	https://esgf-node.llnl.gov/search/cmip6/ (accessed 28/01/2022)		
	CMIP6 data citations							
	GFDL-ESM4: hist-piAer, histSST, histSST-piAer, historical	Input dataset			Horowitz et al. (2018a, b, c, d)	https://esgf-node.llnl.gov/search/cmip6/ (accessed 28/01/2022)		
	GISS-E2-1-G: hist-piAer, histSST, histSST-piAer, historical	Input dataset			NASA Goddard Institute for Space Studies (NASA/GISS) (2019a, b, c, d)	https://esgf-node.llnl.gov/search/cmip6/ (accessed 28/01/2022)		
	MIROC6: hist-piAer, histSST, histSST-piAer, historical	Input dataset			Takemura (2019a, b, c, d)	https://esgf-node.llnl.gov/search/cmip6/ (accessed 28/01/2022)		
	MRI-ESM2-0: hist-piAer, histSST, histSST-piAer, historical	Input dataset			Yukimoto et al. (2019a, b, 2020a, b)	https://esgf-node.llnl.gov/search/cmip6/ (accessed 28/01/2022)		

Figure Number	Dataset Name	Type of Dataset	File Name	License Type	Dataset Citation	Dataset DOI/URL	Citation for Relevant Papers	Notes
Figure 6.13 (continued)	NorESM2-LM: hist-piAer, histSST, histSST-piAer, historical	Input dataset			Olivière et al. (2019a, b, c, d)	https://esgf-node.llnl.gov/search/cmip6/ (accessed 28/01/2022)		
	UKESM1-0-LL: hist-piAer, histSST, histSST-piAer, historical	Input dataset			O'Connor (2019a, b, c, d)	https://esgf-node.llnl.gov/search/cmip6/ (accessed 28/01/2022)		
Figure 6.14	CMIP6 historical experiment, AerChemMIP experiments ssp370, ssp370SST, ssp370pdSST experiments. Output variables: o3, tas	Input dataset Monthly mean	Models: GFDL-ESM4, GISS-E2-1-G, MRI-ESM2-0, UKESM1-0-LL	Public https://esgf.llnl.gov/LICENSE.html	Eyring et al. (2016); Collins et al. (2017)	https://esgf-node.llnl.gov/search/cmip6/ (accessed 28/01/2022)		
	CMIP6 data citations							
	GFDL-ESM4: ssp370SST, ssp370pdSST	Input dataset			Horowitz et al. (2018g, h)	https://esgf-node.llnl.gov/search/cmip6/ (accessed 28/01/2022)		
	GISS-E2-1-G: ssp370SST, ssp370pdSST	Input dataset			NASA Goddard Institute for Space Studies (NASA/GISS) (2020c, d)	https://esgf-node.llnl.gov/search/cmip6/ (accessed 28/01/2022)		
	MRI-ESM2-0: ssp370SST, ssp370pdSST	Input dataset			Yukimoto et al. (2019d, 2020d)	https://esgf-node.llnl.gov/search/cmip6/ (accessed 28/01/2022)		
Figure 6.15	CMIP6, ScenarioMIP experiments ssp370SST, ssp370pdSST.	Input dataset				https://esgf-node.llnl.gov/search/cmip6/ (accessed 28/01/2022)		See IPCC AR6 WGI 6.SM.1, 6.SM.2 for details
Figure 6.16	Community Emissions Data System (CEDS) for Historical Emissions GAINS model	Code	CMIP6 Data Release (data only) July 26, 2016 for CEDS ECLIPSE version 6b	Open Source	Klimont et al. (2017) Lee et al. (2020); Purohit et al. (2020); van Marle et al. (2017)	www.globalchange.umd.edu/ceds/ (accessed 28/01/2022) https://github.com/JGCRI/CEDS/ (accessed 28/01/2022) https://iiasa.ac.at/web/home/research/researchPrograms/air/Global_emissions.html (accessed 28/01/2022)		See IPCC AR6 WGI 6.SM.4 for details
Figure 6.17	TM5-FASST model Community Emissions Data System (CEDS) for Historical Emissions CAMS global reanalysis (EAC4)	Input Dataset Input Dataset Code	CMIP6 Data Release (data only) July 26, 2016 for CEDS	Open Source https://apps.ecmwf.int/datasets/licences/copernicus/	Van Dingenen et al. (2018) Inness et al. (2019)	www.globalchange.umd.edu/ceds/ (accessed 28/01/2022) https://github.com/JGCRI/CEDS/ (accessed 28/01/2022) www.ecmwf.int/en/forecasts/dataset/cams-global-reanalysis (accessed 28/01/2022)	Hoesly et al. (2018)	

Figure Number	Dataset Name	Type of Dataset	File Name	License Type	Dataset Citation	Dataset DOI/URL	Citation for Relevant Papers	Notes
Figure 6.18	GEIA/ACCENT gridded emissions	Input dataset		Public		http://geiacenter.org (accessed 28/01/2022)	Lamarque et al. (2010)	
	Community Emissions Data System (CEDS) for Historical Emissions	Input dataset	Gmd-11- 369-2018-supplement input4MIPs. CMIP6.CMIP .VUA.VUA- CMIP-BB4CMIP6- 1-2	Public	Hoesly et al. (2018); van Marle et al. (2017)	www.globalchange.umd.edu/ceds/ (accessed 28/01/2022) https://github.com/JGCRI/CEDS/ (accessed 28/01/2022) http://esgf-node.llnl.gov/search/input4mips/ (accessed 28/01/2022)		
			CMIP6 Data Release (data only) July 26, 2016 for CEDS					
	EDGAR 5.0	Input dataset		Public	Crippa et al., (2019b, 2020)	https://edgar.jrc.ec.europa.eu/ (accessed 28/01/2022) https://edgar.jrc.ec.europa.eu/dataset_ap50 (accessed 28/01/2022)		
	ECLIPSE	Input dataset	ECLIPSE_v5a	Public	Klimont et al. (2017) Stohl et al. (2015)	https://iiasa.ac.at/web/home/research/researchPrograms/air/Global_emissions.html (accessed 28/01/2022) https://iiasa.ac.at/web/home/research/researchPrograms/air/ECLIPSEv5a.html (accessed 28/01/2022)		
	SSP Database (Shared Socioeconomic Pathways) – Version 2.0	Input dataset	SSP_CMIP6_201811.csv.zip	Public	Gidden et al. (2019); Riahi et al. (2017); Rogelj et al. (2018)	https://tntcat.iiasa.ac.at/SspDb/dsd (accessed 28/01/2022)		
Figure 6.19	GEIA/ACCENT gridded emissions	Input dataset		Public		http://geiacenter.org (accessed 28/01/2022)	Lamarque et al. (2010)	
	Community Emissions Data System (CEDS) for Historical Emissions	Input dataset	Gmd-11- 369-2018-supplement input4MIPs. CMIP6.CMIP .VUA.VUA- CMIP-BB4CMIP6- 1-2	Public	Hoesly et al. (2018); van Marle et al. (2017)	http://www.globalchange.umd.edu/ceds/ (accessed 28/01/2022) https://github.com/JGCRI/CEDS/ (accessed 28/01/2022)		
			.VUA.VUA- CMIP-BB4CMIP6- 1-2			http://esgf-node.llnl.gov/search/input4mips/ (accessed 28/01/2022)		
			CMIP6 Data Release (data only) July 26, 2016 for CEDS					

Figure Number	Dataset Name	Type of Dataset	File Name	License Type	Dataset Citation	Dataset DOI/URL	Citation for Relevant Papers	Notes
Figure 6.19 (continued)	SSP Database (Shared Socio-economic Pathways) – Version 2.0	Input dataset	SSP_CMIP6_201811.csv.zip	Public	Gidden et al. (2019); Riahi et al. (2017); Rogelj et al. (2018)	https://tntcat.iiasa.ac.at/SspDb/dsd (accessed 28/01/2022)		
	Representative Concentration Pathway (RCP) database	Input dataset	Direct from website	Public	van Vuuren et al. (2011)	https://tntcat.iiasa.ac.at/RcpDb/dsd (accessed 28/01/2022)		
	Figure 6.19 code	Code				https://github.com/gidden/ar6-wg1-ch6-emissions (accessed 28/01/2022)		
Figures 6.20 and 6.21	GEIA/ACCENT gridded emissions	Input dataset		Public		http://geiacenter.org (accessed 28/01/2022)	Lamarque et al. (2010)	
	Community Emissions Data System (CEDS) for historical emissions	Input dataset		Public	van Marle et al. (2017); Hoesly et al. (2018)	http://www.globalchange.umd.edu/ceds/ (accessed 28/01/2022) http://esgf-node.llnl.gov/search/input4mips/ (accessed 28/01/2022)		
	SSP Database (Shared Socio-economic Pathways) – version 2.0	Input dataset		Public	Riahi et al. (2017); Rogelj et al. (2018); Gidden et al. (2019)	https://tntcat.iiasa.ac.at/SspDb/dsd (accessed 28/01/2022)		
	Representative Concentration Pathway (RCP) database	Input dataset		Public	van Vuuren et al. (2011)			
		Intermediate dataset				https://github.com/gidden/ar6-wg1-ch6-emissions (accessed 28/01/2022) Code: https://github.com/IPCC-WG1/Chapter-6		
	CMIP6 data citations for Figure 6.20							
	EC-Earth3-AerChem: ssp370-lowNTCF, ssp370-lowNTCFCH4, historical, ssp370	Input dataset			EC-Earth Consortium (EC-Earth) (2020b, c, d, e)	https://esgf-node.llnl.gov/search/cmip6/ (accessed 28/01/2022)		
	GFDL-ESM4: ssp370-lowNTCF, ssp370-lowNTCFCH4, historical, ssp126, ssp245, ssp370, ssp585	Input dataset			Horowitz et al. (2018e, f); John et al. (2018a, b, c, d); Krasting et al. (2018b)	https://esgf-node.llnl.gov/search/cmip6/ (accessed 28/01/2022)		
	GISS-E2-1-G: ssp370-lowNTCFCH4, historical, ssp126, ssp245, ssp370, ssp370-lowNTCF, ssp585	Input dataset			NASA Goddard Institute for Space Studies (NASA/GISS) (2018, 2020b, f, g, h, i, j)	https://esgf-node.llnl.gov/search/cmip6/ (accessed 28/01/2022)		

Figure Number	Dataset Name	Type of Dataset	File Name	License Type	Dataset Citation	Dataset DOI/URL	Citation for Relevant Papers	Notes
Figures 6.20 and 6.21 (continued)	MRI-ESM2-0: ssp370-lowNTCFCH4, historical, ssp126, ssp245, ssp370, ssp370-lowNTCF, ssp585	Input dataset			Yukimoto et al. (2019e, g, h, i, j, k, 2020c)	https://esgf-node.llnl.gov/search/cmip6/ (accessed 28/01/2022)		
	UKESM1-0-LL: ssp370-lowNTCFCH4, ssp370-lowNTCF, historical, ssp126, ssp245, ssp370, ssp585	Input dataset			Good et al. (2019a, b, c, d); Tang et al. (2019); Byun (2020); O'Connor (2020a)	https://esgf-node.llnl.gov/search/cmip6/ (accessed 28/01/2022)		
	CMIP6 data citations for Figure 6.21							
	EC-Earth3-AerChem: ssp370-lowNTCF, ssp370-lowNTCFCH4, historical, ssp370	Input dataset			EC-Earth Consortium (EC-Earth) (2020b, c, d, e)	https://esgf-node.llnl.gov/search/cmip6/ (accessed 28/01/2022)		
	GFDL-ESM4: ssp370-lowNTCF, ssp370-lowNTCFCH4, historical, ssp126, ssp245, ssp370, ssp585	Input dataset			Horowitz et al. (2018e, f); John et al. (2018a, b, c, d); Krasting et al. (2018b)	https://esgf-node.llnl.gov/search/cmip6/ (accessed 28/01/2022)		
	GISS-E2-1-G: ssp370-lowNTCF, ssp370-lowNTCFCH4, historical, ssp126, ssp245, ssp370, ssp585	Input dataset			NASA Goddard Institute for Space Studies (NASA/GISS) (2018, 2020a, b, g, h, i, j)	https://esgf-node.llnl.gov/search/cmip6/ (accessed 28/01/2022)		
	MRI-ESM2-0: ssp370-lowNTCF, ssp370-lowNTCFCH4, historical, ssp126, ssp245, ssp370, ssp585	Input dataset			Yukimoto et al. (2019c, e, h, i, j, k, 2020c)	https://esgf-node.llnl.gov/search/cmip6/ (accessed 28/01/2022)		
Figure 6.22	UKESM1-0-LL: ssp370-lowNTCFCH4, ssp370-lowNTCF, historical, ssp126, ssp245, ssp370, ssp585	Input dataset			Good et al. (2019a, b, c, d); Tang et al. (2019); Byun (2020); O'Connor (2020a)	https://esgf-node.llnl.gov/search/cmip6/ (accessed 28/01/2022)		
	NorESM2-LM: ssp370-lowNTCF, historical, ssp126, ssp245, ssp370, ssp585	Input dataset			Oliviè et al. (2019e); Seland et al. (2019a, b, c, d, e)	https://esgf-node.llnl.gov/search/cmip6/ (accessed 28/01/2022)		
Figure 6.23	UKESM1-0-LL: ssp370-lowNTCF, historical, ssp126, ssp245, ssp370, ssp585	Input dataset			Good et al. (2019a, b, c, d); Tang et al. (2019); Byun (2020)	https://esgf-node.llnl.gov/search/cmip6/ (accessed 28/01/2022)		
Figure 6.24	CMIP6, AerChemMIP Output variables: rsut and rlut, monthly output. Ssp370SST and ssp370SST-lowNTCF	Input dataset	BCC-ESM1, CNRM-ESM2-1, CESM2-WACCM and GFDL-ESM4.	Public	Eyring et al. (2016); Collins et al. (2017)	https://esgf-node.llnl.gov/search/cmip6/ (accessed 28/01/2022)		

Figure Number	Dataset Name	Type of Dataset	File Name	License Type	Dataset Citation	Dataset DOI/URL	Citation for Relevant Papers	Notes
Figure 6.25	ScenarioMIP, RCMIP Emulator output	Input dataset		Public	Eyring et al. (2016); O'Neill et al. (2016); Nicholls et al. (2020)	https://esgf-node.llnl.gov/search/cmip6/ (accessed 28/01/2022) https://tntcat.iiasa.ac.at/SspDb/dsd (accessed 28/01/2022)	Geoffroy et al. (2013)	
Figure 6.26	Shared Socio-Economic Pathway (SSP) database	Input dataset			Gidden et al. (2019); Riahi et al. (2017); Rogelj et al. (2018)	https://tntcat.iiasa.ac.at/SspDb/dsd (accessed 28/01/2022)	Rao et al. (2017); Riahi et al. (2017)	
	ScenarioMIP Emulator output	Input dataset		Public	O'Neill et al. (2016)	https://esgf-node.llnl.gov/search/cmip6/ (accessed 28/01/2022)	Lund et al. (2020)	
CMIP6 data citations								
Cross-Chapter Box 6.1, Figure 1	ACCESS-ESM1-5: ssp245-covid	Input dataset			Ziehn et al. (2020)	https://esgf-node.llnl.gov/search/cmip6/ (accessed 28/01/2022)		
	CanESM5: ssp245-covid	Input dataset			Swart et al. (2019)	https://esgf-node.llnl.gov/search/cmip6/ (accessed 28/01/2022)		
	EC-Earth3: ssp245-covid	Input dataset			EC-Earth Consortium (EC-Earth) (2020a)	https://esgf-node.llnl.gov/search/cmip6/ (accessed 28/01/2022)		
	GISS-E2-1-G: ssp245-covid	Input dataset			NASA Goddard Institute for Space Studies (NASA/GISS) (2020e)	https://esgf-node.llnl.gov/search/cmip6/ (accessed 28/01/2022)		
	MIROC-ES2L: ssp245-covid	Input dataset			Ohgaito et al. (2020)	https://esgf-node.llnl.gov/search/cmip6/ (accessed 28/01/2022)		
	MPI-ESM1-2-LR: ssp245-covid	Input dataset			Müller et al. (2019)	https://esgf-node.llnl.gov/search/cmip6/ (accessed 28/01/2022)		
	MRI-ESM2-0: ssp245-covid	Input dataset			Yukimoto et al. (2019f)	https://esgf-node.llnl.gov/search/cmip6/ (accessed 28/01/2022)		
	UKESM1-0-LL: ssp245-covid	Input dataset			Rumbold et al. (2020)	https://esgf-node.llnl.gov/search/cmip6/ (accessed 28/01/2022)		

Figure Number	Dataset Name	Type of Dataset	File Name	License Type	Dataset Citation	Dataset DOI/URL	Citation for Relevant Papers	Notes
Figure 6.SM.1	CMIP6 data citations							
	GFDL-ESM4: ssp370SST, ssp370pdSST	Input dataset			Horowitz et al. (2018g, h)	https://esgf-node.llnl.gov/search/cmip6/ (accessed 28/01/2022)		
	GISS-E2-1-G: ssp370SST, ssp370pdSST	Input dataset			NASA Goddard Institute for Space Studies (NASA/GISS) (2020c, d)	https://esgf-node.llnl.gov/search/cmip6/ (accessed 28/01/2022)		
	MRI-ESM2-0: ssp370SST, ssp370pdSST	Input dataset			Yukimoto et al. (2019d, 2020d)	https://esgf-node.llnl.gov/search/cmip6/ (accessed 28/01/2022)		
	UKESM1-0-LL: ssp370pdSST, ssp370SST	Input dataset			O'Connor (2020b, c)	https://esgf-node.llnl.gov/search/cmip6/ (accessed 28/01/2022)		
Figure 6.SM.2	CMIP6 data citations							
	GFDL-ESM4: ssp370SST, ssp370pdSST	Input dataset			Horowitz et al. (2018g, h)	https://esgf-node.llnl.gov/search/cmip6/ (accessed 28/01/2022)		
	GISS-E2-1-G: ssp370SST, ssp370pdSST	Input dataset			NASA Goddard Institute for Space Studies (NASA/GISS) (2020c, d)	https://esgf-node.llnl.gov/search/cmip6/ (accessed 28/01/2022)		
	MRI-ESM2-0: ssp370SST, ssp370pdSST	Input dataset			Yukimoto et al. (2019d, 2020d)	https://esgf-node.llnl.gov/search/cmip6/ (accessed 28/01/2022)		
Figure 6.SM.3	Community Emissions Data System (CEDS) for Historical Emissions	Input dataset	CMIP6 Data Release (data only) July 26, 2016 for CEDS	Open Source		http://www.globalchange.umd.edu/ceds/ (accessed 28/01/2022) https://github.com/JCRI/CEDS/ (accessed 28/01/2022)	Hoesly et al. (2018)	

Figure Number	Dataset Name	Type of Dataset	File Name	License Type	Dataset Citation	Dataset DOI/URL	Citation for Relevant Papers	Notes
CMIP6 data citations								
Figure 6.SM.4	EC-Earth3-AerChem: ssp370-lowNTCF, ssp370-lowNTCFCH4, historical, ssp370	Input dataset			EC-Earth Consortium (EC-Earth) (2020b, c, d, e)	https://esgf-node.llnl.gov/search/cmip6/ (accessed 28/01/2022)		
	GFDL-ESM4: ssp370-lowNTCF, ssp370-lowNTCFCH4, historical, ssp126, ssp245, ssp370, ssp585	Input dataset			Horowitz et al. (2018e, f); John et al. (2018a, b, c, d); Krasting et al. (2018b)	https://esgf-node.llnl.gov/search/cmip6/ (accessed 28/01/2022)		
	GISS-E2-1-G: ssp370-lowNTCF, ssp370-lowNTCFCH4, historical, ssp126, ssp245, ssp370, ssp585	Input dataset			NASA Goddard Institute for Space Studies (NASA/GISS) (2018, 2020a, b, g, h, i, j)	https://esgf-node.llnl.gov/search/cmip6/ (accessed 28/01/2022)		
	MRI-ESM2-0: ssp370-lowNTCF, ssp370-lowNTCFCH4, historical, ssp126, ssp245, ssp370, ssp585	Input dataset			Yukimoto et al. (2019c, e, h, i, j, k, 2020c)	https://esgf-node.llnl.gov/search/cmip6/ (accessed 28/01/2022)		
	UKESM1-0-LL: ssp370-lowNTCFCH4, ssp370-lowNTCF, historical, ssp126, ssp245, ssp370, ssp585	Input dataset			Good et al. (2019a, b, c, d); Tang et al. (2019); Byun (2020); O'Connor (2020a)	https://esgf-node.llnl.gov/search/cmip6/ (accessed 28/01/2022)		
CMIP6 data citations								
Figure 6.SM.5	EC-Earth3-AerChem: ssp370-lowNTCF, ssp370-lowNTCFCH4, historical, ssp370	Input dataset			EC-Earth Consortium (EC-Earth) (2020b, c, d, e)	https://esgf-node.llnl.gov/search/cmip6/ (accessed 28/01/2022)		
	GFDL-ESM4: ssp370-lowNTCF, ssp370-lowNTCFCH4, historical, ssp126, ssp245, ssp370, ssp585	Input dataset			Horowitz et al. (2018e, f); John et al. (2018a, b, c, d); Krasting et al. (2018b)	https://esgf-node.llnl.gov/search/cmip6/ (accessed 28/01/2022)		
	GISS-E2-1-G: ssp370-lowNTCFCH4, historical, ssp126, ssp245, ssp370, ssp370-lowNTCF, ssp585	Input dataset			NASA Goddard Institute for Space Studies (NASA/GISS) (2018, 2020b, f, g, h, i, j)	https://esgf-node.llnl.gov/search/cmip6/ (accessed 28/01/2022)		
	MRI-ESM2-0: ssp370-lowNTCFCH4, historical, ssp126, ssp245, ssp370, ssp370-lowNTCF, ssp585	Input dataset			Yukimoto et al. (2019e, g, h, i, j, k, 2020c)	https://esgf-node.llnl.gov/search/cmip6/ (accessed 28/01/2022)		
	UKESM1-0-LL: ssp370-lowNTCFCH4, ssp370-lowNTCF, historical, ssp126, ssp245, ssp370, ssp585	Input dataset			Good et al. (2019a, b, c, d); Tang et al. (2019); Byun (2020); O'Connor (2020a)	https://esgf-node.llnl.gov/search/cmip6/ (accessed 28/01/2022)		

References

- Aakre, S., S. Kallbekken, R. Van Dingenen, and D.G. Victor, 2018: Incentives for small clubs of Arctic countries to limit black carbon and methane emissions. *Nature Climate Change*, **8**(1), 85–90, doi:[10.1038/s41558-017-0030-8](https://doi.org/10.1038/s41558-017-0030-8).
- Aggarwal, S.G. and K. Kawamura, 2009: Carbonaceous and inorganic composition in long-range transported aerosols over northern Japan: Implication for aging of water-soluble organic fraction. *Atmospheric Environment*, **43**(16), 2532–2540, doi:[10.1016/j.atmosenv.2009.02.032](https://doi.org/10.1016/j.atmosenv.2009.02.032).
- Batmunkh,T. et.al., 2011: Time-Resolved Measurements of PM_{2.5} Carbonaceous Aerosols at Gosan, Korea. *Journal of the Air & Waste Management Association*, **61**(11), 1174–1182, doi:[10.1080/10473289.2011.609761](https://doi.org/10.1080/10473289.2011.609761).
- Bourrotte, C. et al., 2007: Association between ionic composition of fine and coarse aerosol soluble fraction and peak expiratory flow of asthmatic patients in São Paulo city (Brazil). *Atmospheric Environment*, **41**(10), 2036–2048, doi:[10.1016/j.atmosenv.2006.11.004](https://doi.org/10.1016/j.atmosenv.2006.11.004).
- Brauer, M. et al., 2016: Ambient Air Pollution Exposure Estimation for the Global Burden of Disease 2013. *Environmental Science & Technology*, **50**(1), 79–88, doi:[10.1021/acs.est.5b03709](https://doi.org/10.1021/acs.est.5b03709).
- Byun, Y.-H., 2020: NIMS-KMA UKESM1.0-LL model output prepared for CMIP6 AerChemMIP ssp370-lowNTCF. Earth System Grid Federation, doi:[10.22033/esgf/cmip6.8440](https://doi.org/10.22033/esgf/cmip6.8440).
- Celis, J.E., J.R. Morales, C.A. Zaror, and J.C. Inzunza, 2004: A study of the particulate matter PM10 composition in the atmosphere of Chillán, Chile. *Chemosphere*, **54**(4), 541–550, doi:[10.1016/s0045-6535\(03\)00711-2](https://doi.org/10.1016/s0045-6535(03)00711-2).
- Cho, S.Y. and S.S. Park, 2013: Resolving sources of water-soluble organic carbon in fine particulate matter measured at an urban site during winter. *Environmental Science: Processes & Impacts*, **15**, 524–534, doi:[10.1039/c2em30730h](https://doi.org/10.1039/c2em30730h).
- Collins, W.J. et al., 2017: AerChemMIP: Quantifying the effects of chemistry and aerosols in CMIP6. *Geoscientific Model Development*, **10**(2), 585–607, doi:[10.5194/gmd-10-585-2017](https://doi.org/10.5194/gmd-10-585-2017).
- Cooper, O.R. et al., 2020: Multi-decadal surface ozone trends at globally distributed remote locations. *Elementa: Science of the Anthropocene*, **8**(1), 23, doi:[10.1525/elementa.420](https://doi.org/10.1525/elementa.420).
- Crippa, M., G. Janssens-Maenhout, D. Guizzardi, R. Van Dingenen, and F. Dentener, 2019: Contribution and uncertainty of sectorial and regional emissions to regional and global PM2.5 health impacts. *Atmospheric Chemistry and Physics*, **19**(7), 5165–5186, doi:[10.5194/acp-19-5165-2019](https://doi.org/10.5194/acp-19-5165-2019).
- Danabasoglu, G., 2019a: NCAR CESM2-WACCM model output prepared for CMIP6 CMIP historical. Earth System Grid Federation, doi:[10.22033/esgf/cmip6.10071](https://doi.org/10.22033/esgf/cmip6.10071).
- Danabasoglu, G., 2019b: NCAR CESM2-WACCM model output prepared for CMIP6 ScenarioMIP ssp370. Earth System Grid Federation, doi:[10.22033/esgf/cmip6.10102](https://doi.org/10.22033/esgf/cmip6.10102).
- de Souza, P.A., W.Z. Mello, R.L. Mariani, and S.M. Sella, 2010: Caracterização do material particulado fino e grosso e composição da fração inorgânica solúvel em água em São José dos Campos (SP). *Química Nova*, **33**(6), 1247–1253.
- EC-Earth Consortium (EC-Earth), 2020a: EC-Earth-Consortium EC-Earth3 model output prepared for CMIP6 DAMIP ssp245-covid. Earth System Grid Federation, doi:[10.22033/esgf/cmip6.14943](https://doi.org/10.22033/esgf/cmip6.14943).
- EC-Earth Consortium (EC-Earth), 2020b: EC-Earth-Consortium EC-Earth3-AerChem model output prepared for CMIP6 AerChemMIP ssp370-lowNTCF. Earth System Grid Federation, doi:[10.22033/esgf/cmip6.4889](https://doi.org/10.22033/esgf/cmip6.4889).
- EC-Earth Consortium (EC-Earth), 2020c: EC-Earth-Consortium EC-Earth3-AerChem model output prepared for CMIP6 AerChemMIP ssp370-lowNTCFCH4. Earth System Grid Federation, doi:[10.22033/esgf/cmip6.13515](https://doi.org/10.22033/esgf/cmip6.13515).
- EC-Earth Consortium (EC-Earth), 2020d: EC-Earth-Consortium EC-Earth3-AerChem model output prepared for CMIP6 CMIP historical. Earth System Grid Federation, doi:[10.22033/esgf/cmip6.4701](https://doi.org/10.22033/esgf/cmip6.4701).
- EC-Earth Consortium (EC-Earth), 2020e: EC-Earth-Consortium EC-Earth3-AerChem model output prepared for CMIP6 ScenarioMIP ssp370. Earth System Grid Federation, doi:[10.22033/esgf/cmip6.4885](https://doi.org/10.22033/esgf/cmip6.4885).
- Eyring, V. et al., 2016: Overview of the Coupled Model Intercomparison Project Phase 6 (CMIP6) experimental design and organization. *Geoscientific Model Development*, **9**(5), 1937–1958, doi:[10.5194/gmd-9-1937-2016](https://doi.org/10.5194/gmd-9-1937-2016).
- Favez, O. et al., 2008: Seasonality of major aerosol species and their transformations in Cairo megacity. *Atmospheric Environment*, **42**(7), 1503–1516, doi:[10.1016/j.atmosenv.2007.10.081](https://doi.org/10.1016/j.atmosenv.2007.10.081).
- Feng, J. et al., 2006: A comparative study of the organic matter in PM2.5 from three Chinese megalopolises in three different climatic zones. *Atmospheric Environment*, **40**(21), 3983–3994, doi:[10.1016/j.atmosenv.2006.02.017](https://doi.org/10.1016/j.atmosenv.2006.02.017).
- Fuzzi, S. et al., 2007: Overview of the inorganic and organic composition of size-segregated aerosol in Rondônia, Brazil, from the biomass-burning period to the onset of the wet season. *Journal of Geophysical Research: Atmospheres*, **112**(D1), D01201, doi:[10.1029/2005jd006741](https://doi.org/10.1029/2005jd006741).
- Gasser, T. et al., 2017: Accounting for the climate–carbon feedback in emission metrics. *Earth System Dynamics*, **8**(2), 235–253, doi:[10.5194/esd-8-235-2017](https://doi.org/10.5194/esd-8-235-2017).
- Gaudel, A. et al., 2018: Tropospheric Ozone Assessment Report: Present-day distribution and trends of tropospheric ozone relevant to climate and global atmospheric chemistry model evaluation. *Elementa: Science of the Anthropocene*, **6**(1), 39, doi:[10.1525/elementa.291](https://doi.org/10.1525/elementa.291).
- Gaudel, A. et al., 2020: Aircraft observations since the 1990s reveal increases of tropospheric ozone at multiple locations across the Northern Hemisphere. *Science Advances*, **6**(34), eaba8272, doi:[10.1126/sciadv.aba8272](https://doi.org/10.1126/sciadv.aba8272).
- Geoffroy, O. et al., 2013: Transient Climate Response in a Two-Layer Energy-Balance Model. Part I: Analytical Solution and Parameter Calibration Using CMIP5 AOGCM Experiments. *Journal of Climate*, **26**(6), 1841–1857, doi:[10.1175/jcli-d-12-00195.1](https://doi.org/10.1175/jcli-d-12-00195.1).
- Georgoulas, A.K., R.A.J. Van Der, P. Stammes, K. Folkert Boersma, and H.J. Eskes, 2019: Trends and trend reversal detection in 2 decades of tropospheric NO₂ satellite observations. *Atmospheric Chemistry and Physics*, **19**(9), 6269–6294, doi:[10.5194/acp-19-6269-2019](https://doi.org/10.5194/acp-19-6269-2019).
- Gidden, M.J. et al., 2019: Global emissions pathways under different socioeconomic scenarios for use in CMIP6: A dataset of harmonized emissions trajectories through the end of the century. *Geoscientific Model Development*, **12**(4), 1443–1475, doi:[10.5194/gmd-12-1443-2019](https://doi.org/10.5194/gmd-12-1443-2019).
- Gioda, A., B.S. Amaral, I.L.G. Monteiro, and T.D. Saint’Pierre, 2011: Chemical composition, sources, solubility, and transport of aerosol trace elements in a tropical region. *Journal of Environmental Monitoring*, **13**(8), 2134–2142, doi:[10.1039/c1em10240k](https://doi.org/10.1039/c1em10240k).
- Good, P. et al., 2019a: MOHC UKESM1.0-LL model output prepared for CMIP6 ScenarioMIP ssp126. Earth System Grid Federation, doi:[10.22033/esgf/cmip6.6333](https://doi.org/10.22033/esgf/cmip6.6333).
- Good, P. et al., 2019b: MOHC UKESM1.0-LL model output prepared for CMIP6 ScenarioMIP ssp245. Earth System Grid Federation, doi:[10.22033/esgf/cmip6.6339](https://doi.org/10.22033/esgf/cmip6.6339).
- Good, P. et al., 2019c: MOHC UKESM1.0-LL model output prepared for CMIP6 ScenarioMIP ssp370. Earth System Grid Federation, doi:[10.22033/esgf/cmip6.6347](https://doi.org/10.22033/esgf/cmip6.6347).
- Good, P. et al., 2019d: MOHC UKESM1.0-LL model output prepared for CMIP6 ScenarioMIP ssp585. Earth System Grid Federation, doi:[10.22033/esgf/cmip6.6405](https://doi.org/10.22033/esgf/cmip6.6405).
- Harmsen, M.J.H.M. et al., 2020: Co-benefits of black carbon mitigation for climate and air quality. *Climatic Change*, **163**(3), 1519–1538, doi:[10.1007/s10584-020-02800-8](https://doi.org/10.1007/s10584-020-02800-8).

- Hodnebrog et al., 2020: Updated Global Warming Potentials and Radiative Efficiencies of Halocarbons and Other Weak Atmospheric Absorbers. *Reviews of Geophysics*, **58**(3), e2019RG000691, doi:[10.1029/2019rg000691](https://doi.org/10.1029/2019rg000691).
- Hoesly, R.M. et al., 2018: Historical (1750–2014) anthropogenic emissions of reactive gases and aerosols from the Community Emissions Data System (CEDS). *Geoscientific Model Development*, **11**(1), 369–408, doi:[10.5194/gmd-11-369-2018](https://doi.org/10.5194/gmd-11-369-2018).
- Horowitz, L.W. et al., 2018a: NOAA-GFDL GFDL-ESM4 model output prepared for CMIP6 AerChemMIP. Earth System Grid Federation, doi:[10.22033/esgf/cmp6.1404](https://doi.org/10.22033/esgf/cmp6.1404).
- Horowitz, L.W. et al., 2018b: NOAA-GFDL GFDL-ESM4 model output prepared for CMIP6 AerChemMIP hist-piAer. Earth System Grid Federation, doi:[10.22033/esgf/cmp6.8577](https://doi.org/10.22033/esgf/cmp6.8577).
- Horowitz, L.W. et al., 2018c: NOAA-GFDL GFDL-ESM4 model output prepared for CMIP6 AerChemMIP histSST. Earth System Grid Federation, doi:[10.22033/esgf/cmp6.8586](https://doi.org/10.22033/esgf/cmp6.8586).
- Horowitz, L.W. et al., 2018d: NOAA-GFDL GFDL-ESM4 model output prepared for CMIP6 AerChemMIP histSST-piAer. Earth System Grid Federation, doi:[10.22033/esgf/cmp6.8588](https://doi.org/10.22033/esgf/cmp6.8588).
- Horowitz, L.W. et al., 2018e: NOAA-GFDL GFDL-ESM4 model output prepared for CMIP6 AerChemMIP ssp370-lowNTCF. Earth System Grid Federation, doi:[10.22033/esgf/cmp6.8693](https://doi.org/10.22033/esgf/cmp6.8693).
- Horowitz, L.W. et al., 2018f: NOAA-GFDL GFDL-ESM4 model output prepared for CMIP6 AerChemMIP ssp370-lowNTCFCH4. Earth System Grid Federation, doi:[10.22033/esgf/cmp6.13561](https://doi.org/10.22033/esgf/cmp6.13561).
- Horowitz, L.W. et al., 2018g: NOAA-GFDL GFDL-ESM4 model output prepared for CMIP6 AerChemMIP ssp370pdSST. Earth System Grid Federation, doi:[10.22033/esgf/cmp6.11338](https://doi.org/10.22033/esgf/cmp6.11338).
- Horowitz, L.W. et al., 2018h: NOAA-GFDL GFDL-ESM4 model output prepared for CMIP6 AerChemMIP ssp370SST. Earth System Grid Federation, doi:[10.22033/esgf/cmp6.8695](https://doi.org/10.22033/esgf/cmp6.8695).
- John, J.G. et al., 2018a: NOAA-GFDL GFDL-ESM4 model output prepared for CMIP6 ScenarioMIP ssp126. Earth System Grid Federation, doi:[10.22033/esgf/cmp6.8684](https://doi.org/10.22033/esgf/cmp6.8684).
- John, J.G. et al., 2018b: NOAA-GFDL GFDL-ESM4 model output prepared for CMIP6 ScenarioMIP ssp245. Earth System Grid Federation, doi:[10.22033/esgf/cmp6.8686](https://doi.org/10.22033/esgf/cmp6.8686).
- John, J.G. et al., 2018c: NOAA-GFDL GFDL-ESM4 model output prepared for CMIP6 ScenarioMIP ssp370. Earth System Grid Federation, doi:[10.22033/esgf/cmp6.8691](https://doi.org/10.22033/esgf/cmp6.8691).
- John, J.G. et al., 2018d: NOAA-GFDL GFDL-ESM4 model output prepared for CMIP6 ScenarioMIP ssp585. Earth System Grid Federation, doi:[10.22033/esgf/cmp6.8706](https://doi.org/10.22033/esgf/cmp6.8706).
- Joos, F. et al., 2013: Carbon dioxide and climate impulse response functions for the computation of greenhouse gas metrics: a multi-model analysis. *Atmospheric Chemistry and Physics*, **13**(5), 2793–2825, doi:[10.5194/acp-13-2793-2013](https://doi.org/10.5194/acp-13-2793-2013).
- Karagulian, F. et al., 2016: Attribution of anthropogenic PM_{2.5} to emission sources: A global analysis of source-receptor model results and measured source-apportionment data (No. EUR 28510 EN), JRC Technical Reports, 1–43.
- Krasting, J.P. et al., 2018a: NOAA-GFDL GFDL-ESM4 model output prepared for CMIP6 CMIP esm-hist. Earth System Grid Federation, doi:[10.22033/esgf/cmp6.8522](https://doi.org/10.22033/esgf/cmp6.8522).
- Krasting, J.P. et al., 2018b: NOAA-GFDL GFDL-ESM4 model output prepared for CMIP6 CMIP historical. Earth System Grid Federation, doi:[10.22033/esgf/cmp6.8597](https://doi.org/10.22033/esgf/cmp6.8597).
- Kühn, T. et al., 2020: Effects of black carbon mitigation on Arctic climate. *Atmospheric Chemistry and Physics*, **20**(9), 5527–5546, doi:[10.5194/acp-20-5527-2020](https://doi.org/10.5194/acp-20-5527-2020).
- Kuzu, S.L. et al., 2020: Black carbon and size-segregated elemental carbon, organic carbon compositions in a megacity: a case study for Istanbul. *Air Quality, Atmosphere & Health*, **13**(7), 827–837, doi:[10.1007/s11869-020-00839-1](https://doi.org/10.1007/s11869-020-00839-1).
- Lamarque, J.F. et al., 2010: Historical (1850–2000) gridded anthropogenic and biomass burning emissions of reactive gases and aerosols: Methodology and application. *Atmospheric Chemistry and Physics*, **10**(15), 7017–7039, doi:[10.5194/acp-10-7017-2010](https://doi.org/10.5194/acp-10-7017-2010).
- Lee, D.S. et al., 2021: The contribution of global aviation to anthropogenic climate forcing for 2000 to 2018. *Atmospheric Environment*, **244**, 117834, doi:[10.1016/j.atmosenv.2020.117834](https://doi.org/10.1016/j.atmosenv.2020.117834).
- Li, L. et al., 2010: Composition, source, mass closure of PM_{2.5} aerosols for four forests in eastern China. *Journal of Environmental Sciences*, **22**(3), 405–412, doi:[10.1016/s1001-0742\(09\)60122-4](https://doi.org/10.1016/s1001-0742(09)60122-4).
- Lund, M.T. et al., 2020: A continued role of short-lived climate forcers under the Shared Socioeconomic Pathways. *Earth System Dynamics*, **11**(4), 977–993, doi:[10.5194/esd-11-977-2020](https://doi.org/10.5194/esd-11-977-2020).
- Mariani, R.L. and W.Z. de Mello, 2007: PM_{2.5}-10, PM_{2.5} and associated water-soluble inorganic species at a coastal urban site in the metropolitan region of Rio de Janeiro. *Atmospheric Environment*, **41**(13), 2887–2892, doi:[10.1016/j.atmosenv.2006.12.009](https://doi.org/10.1016/j.atmosenv.2006.12.009).
- Markandya, A. et al., 2018: Health co-benefits from air pollution and mitigation costs of the Paris Agreement: a modelling study. *The Lancet Planetary Health*, **2**(3), e126–e133, doi:[10.1016/s2542-5196\(18\)30029-9](https://doi.org/10.1016/s2542-5196(18)30029-9).
- Martin, S.T. et al., 2010: Sources and properties of Amazonian aerosol particles. *Reviews of Geophysics*, **48**(2), RG2002, doi:[10.1029/2008rg000280](https://doi.org/10.1029/2008rg000280).
- Mkoma, S.L., 2008: Physico-Chemical Characterisation of Atmospheric Aerosols in Tanzania, with Emphasis on the Carbonaceous Aerosol Components and on Chemical Mass Closure., Ghent University, Faculty of Sciences, Ghent, Belgium, 182 pp., doi:[10.1016/j.atmosenv.2008.10.008](https://doi.org/10.1016/j.atmosenv.2008.10.008).
- Mkoma, S.L., W. Maenhaut, X. Chi, W. Wang, and N. Raes, 2009: Characterisation of PM₁₀ atmospheric aerosols for the wet season 2005 at two sites in East Africa. *Atmospheric Environment*, **43**(3), 631–639, doi:[10.1016/j.atmosenv.2008.10.008](https://doi.org/10.1016/j.atmosenv.2008.10.008).
- Molina, L.T. et al., 2007: Air quality in North America's most populous city – overview of the MCMA-2003 campaign. *Atmospheric Chemistry and Physics*, **7**(10), 2447–2473, doi:[10.5194/acp-7-2447-2007](https://doi.org/10.5194/acp-7-2447-2007).
- Molina, L.T. et al., 2010: An overview of the MILAGRO 2006 Campaign: Mexico City emissions and their transport and transformation. *Atmospheric Chemistry and Physics*, **10**(18), 8697–8760, doi:[10.5194/acp-10-8697-2010](https://doi.org/10.5194/acp-10-8697-2010).
- Montzka, S.A. et al., 2011: Small Interannual Variability of Global Atmospheric Hydroxyl. *Science*, **331**(6013), 67–69, doi:[10.1126/science.1197640](https://doi.org/10.1126/science.1197640).
- Müller, W. et al., 2019: MPI-M MPI-ESM1.2-LR model output prepared for CMIP6 DAMIP ssp245-covid. Earth System Grid Federation, doi:[10.22033/esgf/cmp6.15041](https://doi.org/10.22033/esgf/cmp6.15041).
- NASA Goddard Institute for Space Studies (NASA/GISS), 2018: NASA-GISS GISS-E2.1G model output prepared for CMIP6 CMIP historical. Earth System Grid Federation, doi:[10.22033/esgf/cmp6.7127](https://doi.org/10.22033/esgf/cmp6.7127).
- NASA Goddard Institute for Space Studies (NASA/GISS), 2019a: NASA-GISS GISS-E2.1G model output prepared for CMIP6 AerChemMIP. Earth System Grid Federation, doi:[10.22033/esgf/cmp6.2059](https://doi.org/10.22033/esgf/cmp6.2059).
- NASA Goddard Institute for Space Studies (NASA/GISS), 2019b: NASA-GISS GISS-E2.1G model output prepared for CMIP6 AerChemMIP hist-piAer. Earth System Grid Federation, doi:[10.22033/esgf/cmp6.7093](https://doi.org/10.22033/esgf/cmp6.7093).
- NASA Goddard Institute for Space Studies (NASA/GISS), 2019c: NASA-GISS GISS-E2.1G model output prepared for CMIP6 AerChemMIP histSST. Earth System Grid Federation, doi:[10.22033/esgf/cmp6.7113](https://doi.org/10.22033/esgf/cmp6.7113).
- NASA Goddard Institute for Space Studies (NASA/GISS), 2019d: NASA-GISS GISS-E2.1G model output prepared for CMIP6 AerChemMIP histSST-piAer. Earth System Grid Federation, doi:[10.22033/esgf/cmp6.7117](https://doi.org/10.22033/esgf/cmp6.7117).
- NASA Goddard Institute for Space Studies (NASA/GISS), 2020a: NASA-GISS GISS-E2.1G model output prepared for CMIP6 AerChemMIP ssp370-lowNTCF. Earth System Grid Federation, doi:[10.22033/esgf/cmp6.7431](https://doi.org/10.22033/esgf/cmp6.7431).
- NASA Goddard Institute for Space Studies (NASA/GISS), 2020b: NASA-GISS GISS-E2.1G model output prepared for CMIP6 AerChemMIP

- ssp370-lowNTCFCH4. Earth System Grid Federation, doi:[10.22033/esgf/cmip6.13531](https://doi.org/10.22033/esgf/cmip6.13531).
- NASA Goddard Institute for Space Studies (NASA/GISS), 2020c: NASA-GISS GISS-E2.1G model output prepared for CMIP6 AerChemMIP ssp370pdSSST. Earth System Grid Federation, doi:[10.22033/esgf/cmip6.11387](https://doi.org/10.22033/esgf/cmip6.11387).
- NASA Goddard Institute for Space Studies (NASA/GISS), 2020d: NASA-GISS GISS-E2.1G model output prepared for CMIP6 AerChemMIP ssp370SST. Earth System Grid Federation, doi:[10.22033/esgf/cmip6.7435](https://doi.org/10.22033/esgf/cmip6.7435).
- NASA Goddard Institute for Space Studies (NASA/GISS), 2020e: NASA-GISS GISS-E2.1G model output prepared for CMIP6 DAMIP ssp245-covid. Earth System Grid Federation, doi:[10.22033/esgf/cmip6.14971](https://doi.org/10.22033/esgf/cmip6.14971).
- NASA Goddard Institute for Space Studies (NASA/GISS), 2020f: NASA-GISS GISS-E2.1G model output prepared for CMIP6 ScenarioMIP. Earth System Grid Federation, doi:[10.22033/esgf/cmip6.2074](https://doi.org/10.22033/esgf/cmip6.2074).
- NASA Goddard Institute for Space Studies (NASA/GISS), 2020g: NASA-GISS GISS-E2.1G model output prepared for CMIP6 ScenarioMIP ssp126. Earth System Grid Federation, doi:[10.22033/esgf/cmip6.7410](https://doi.org/10.22033/esgf/cmip6.7410).
- NASA Goddard Institute for Space Studies (NASA/GISS), 2020h: NASA-GISS GISS-E2.1G model output prepared for CMIP6 ScenarioMIP ssp245. Earth System Grid Federation, doi:[10.22033/esgf/cmip6.7415](https://doi.org/10.22033/esgf/cmip6.7415).
- NASA Goddard Institute for Space Studies (NASA/GISS), 2020i: NASA-GISS GISS-E2.1G model output prepared for CMIP6 ScenarioMIP ssp370. Earth System Grid Federation, doi:[10.22033/esgf/cmip6.7426](https://doi.org/10.22033/esgf/cmip6.7426).
- NASA Goddard Institute for Space Studies (NASA/GISS), 2020j: NASA-GISS GISS-E2.1G model output prepared for CMIP6 ScenarioMIP ssp585. Earth System Grid Federation, doi:[10.22033/esgf/cmip6.7460](https://doi.org/10.22033/esgf/cmip6.7460).
- Naus, S. et al., 2019: Constraints and biases in a tropospheric two-box model of OH. *Atmospheric Chemistry and Physics*, **19**(1), 407–424, doi:[10.5194/acp-19-407-2019](https://doi.org/10.5194/acp-19-407-2019).
- Neubauer, D. et al., 2019a: HAMMOZ-Consortium MPI-ESM1.2-HAM model output prepared for CMIP6 AerChemMIP histSST. Earth System Grid Federation, doi:[10.22033/esgf/cmip6.5009](https://doi.org/10.22033/esgf/cmip6.5009).
- Neubauer, D. et al., 2019b: HAMMOZ-Consortium MPI-ESM1.2-HAM model output prepared for CMIP6 AerChemMIP histSST-piAer. Earth System Grid Federation, doi:[10.22033/esgf/cmip6.5011](https://doi.org/10.22033/esgf/cmip6.5011).
- Nicely, J.M. et al., 2018: Changes in Global Tropospheric OH Expected as a Result of Climate Change Over the Last Several Decades. *Journal of Geophysical Research: Atmospheres*, **123**(18), 10774–10795, doi:[10.1029/2018jd028388](https://doi.org/10.1029/2018jd028388).
- Nicholls, Z.R.J. et al., 2020: Reduced complexity model intercomparison project phase 1: Protocol, results and initial observations. *Geoscientific Model Development*, **13**, 5175–5190, doi:[10.5194/gmd-13-5175-2020](https://doi.org/10.5194/gmd-13-5175-2020).
- O'Connor, F., 2019a: MOHC UKESM1.0-LL model output prepared for CMIP6 AerChemMIP. Earth System Grid Federation, doi:[10.22033/esgf/cmip6.1561](https://doi.org/10.22033/esgf/cmip6.1561).
- O'Connor, F., 2019b: MOHC UKESM1.0-LL model output prepared for CMIP6 AerChemMIP hist-piAer. Earth System Grid Federation, doi:[10.22033/esgf/cmip6.6062](https://doi.org/10.22033/esgf/cmip6.6062).
- O'Connor, F., 2019c: MOHC UKESM1.0-LL model output prepared for CMIP6 AerChemMIP histSST. Earth System Grid Federation, doi:[10.22033/esgf/cmip6.6077](https://doi.org/10.22033/esgf/cmip6.6077).
- O'Connor, F., 2019d: MOHC UKESM1.0-LL model output prepared for CMIP6 AerChemMIP histSST-piAer. Earth System Grid Federation, doi:[10.22033/esgf/cmip6.6085](https://doi.org/10.22033/esgf/cmip6.6085).
- O'Connor, F., 2020a: MOHC UKESM1.0-LL model output prepared for CMIP6 AerChemMIP ssp370-lowNTCFCH4. Earth System Grid Federation, doi:[10.22033/esgf/cmip6.13521](https://doi.org/10.22033/esgf/cmip6.13521).
- O'Connor, F., 2020b: MOHC UKESM1.0-LL model output prepared for CMIP6 AerChemMIP ssp370pdSSST. Earth System Grid Federation, doi:[10.22033/esgf/cmip6.11405](https://doi.org/10.22033/esgf/cmip6.11405).
- O'Connor, F., 2020c: NERC UKESM1.0-LL model output prepared for CMIP6 AerChemMIP ssp370SST. Earth System Grid Federation, doi:[10.22033/esgf/cmip6.6362](https://doi.org/10.22033/esgf/cmip6.6362).
- O'Neill, B.C. et al., 2016: The Scenario Model Intercomparison Project (ScenarioMIP) for CMIP6. *Geoscientific Model Development*, **9**(9), 3461–3482, doi:[10.5194/gmd-9-3461-2016](https://doi.org/10.5194/gmd-9-3461-2016).
- Ohgaito, R. et al., 2020: MIROC MIROC-ES2L model output prepared for CMIP6 DAMIP ssp245-covid. Earth System Grid Federation, doi:[10.22033/esgf/cmip6.15262](https://doi.org/10.22033/esgf/cmip6.15262).
- Oliviè, D.J.L. et al., 2019a: NCC NorESM2-LM model output prepared for CMIP6 AerChemMIP. Earth System Grid Federation, doi:[10.22033/esgf/cmip6.574](https://doi.org/10.22033/esgf/cmip6.574).
- Oliviè, D.J.L. et al., 2019b: NCC NorESM2-LM model output prepared for CMIP6 AerChemMIP hist-piAer. Earth System Grid Federation, doi:[10.22033/esgf/cmip6.7984](https://doi.org/10.22033/esgf/cmip6.7984).
- Oliviè, D.J.L. et al., 2019c: NCC NorESM2-LM model output prepared for CMIP6 AerChemMIP histSST. Earth System Grid Federation, doi:[10.22033/esgf/cmip6.8007](https://doi.org/10.22033/esgf/cmip6.8007).
- Oliviè, D.J.L. et al., 2019d: NCC NorESM2-LM model output prepared for CMIP6 AerChemMIP histSST-piAer. Earth System Grid Federation, doi:[10.22033/esgf/cmip6.8015](https://doi.org/10.22033/esgf/cmip6.8015).
- Oliviè, D.J.L. et al., 2019e: NCC NorESM2-LM model output prepared for CMIP6 AerChemMIP ssp370-lowNTCF. Earth System Grid Federation, doi:[10.22033/esgf/cmip6.8275](https://doi.org/10.22033/esgf/cmip6.8275).
- Pathak, R.K., T. Wang, K.F. Ho, and S.C. Lee, 2011: Characteristics of summertime PM2.5 organic and elemental carbon in four major Chinese cities: Implications of high acidity for water-soluble organic carbon (WSOC). *Atmospheric Environment*, **45**(2), 318–325, doi:[10.1016/j.atmosenv.2010.10.021](https://doi.org/10.1016/j.atmosenv.2010.10.021).
- Patra, P.K. et al., 2021: Methyl Chloroform Continues to Constrain the Hydroxyl (OH) Variability in the Troposphere. *Journal of Geophysical Research: Atmospheres*, **126**(4), e2020JD033862, doi:[10.1029/2020jd033862](https://doi.org/10.1029/2020jd033862).
- Purohit, P. et al., 2020: Electricity savings and greenhouse gas emission reductions from global phase-down of hydrofluorocarbons. *Atmospheric Chemistry and Physics*, **20**(19), 11305–11327, doi:[10.5194/acp-20-11305-2020](https://doi.org/10.5194/acp-20-11305-2020).
- Radhi, M. et al., 2010: Optical, physical and chemical characteristics of Australian continental aerosols: results from a field experiment. *Atmospheric Chemistry and Physics*, **10**(13), 5925–5942, doi:[10.5194/acp-10-5925-2010](https://doi.org/10.5194/acp-10-5925-2010).
- Rao, S. et al., 2017: Future air pollution in the Shared Socio-economic Pathways. *Global Environmental Change*, **42**, 346–358, doi:[10.1016/j.gloenvcha.2016.05.012](https://doi.org/10.1016/j.gloenvcha.2016.05.012).
- Rauner, S. et al., 2020: Coal-exit health and environmental damage reductions outweigh economic impacts. *Nature Climate Change*, **10**(4), 308–312, doi:[10.1038/s41558-020-0728-x](https://doi.org/10.1038/s41558-020-0728-x).
- Riahi, K. et al., 2017: The Shared Socioeconomic Pathways and their energy, land use, and greenhouse gas emissions implications: An overview. *Global Environmental Change*, **42**, 153–168, doi:[10.1016/j.gloenvcha.2016.05.009](https://doi.org/10.1016/j.gloenvcha.2016.05.009).
- Rigby, M. et al., 2017: Role of atmospheric oxidation in recent methane growth. *Proceedings of the National Academy of Sciences*.
- Rogelj, J. et al., 2018: Scenarios towards limiting global mean temperature increase below 1.5°C. *Nature Climate Change*, **8**(4), 325–332, doi:[10.1038/s41558-018-0091-3](https://doi.org/10.1038/s41558-018-0091-3).
- Rumbold, S., J. Walton, and Y. Tang, 2020: MOHC UKESM1.0-LL model output prepared for CMIP6 DAMIP ssp245-covid. Earth System Grid Federation, doi:[10.22033/esgf/cmip6.14884](https://doi.org/10.22033/esgf/cmip6.14884).
- Seland et al., 2019a: NCC NorESM2-LM model output prepared for CMIP6 CMIP historical. Earth System Grid Federation, doi:[10.22033/esgf/cmip6.8036](https://doi.org/10.22033/esgf/cmip6.8036).
- Seland et al., 2019b: NCC NorESM2-LM model output prepared for CMIP6 ScenarioMIP ssp126. Earth System Grid Federation, doi:[10.22033/esgf/cmip6.8248](https://doi.org/10.22033/esgf/cmip6.8248).

- Seland et al., 2019c: NCC NorESM2-LM model output prepared for CMIP6 ScenarioMIP ssp245. Earth System Grid Federation, doi:[10.22033/esgf/cmip6.8253](https://doi.org/10.22033/esgf/cmip6.8253).
- Seland et al., 2019d: NCC NorESM2-LM model output prepared for CMIP6 ScenarioMIP ssp370. Earth System Grid Federation, doi:[10.22033/esgf/cmip6.8268](https://doi.org/10.22033/esgf/cmip6.8268).
- Seland et al., 2019e: NCC NorESM2-LM model output prepared for CMIP6 ScenarioMIP ssp585. Earth System Grid Federation, doi:[10.22033/esgf/cmip6.8319](https://doi.org/10.22033/esgf/cmip6.8319).
- Shine, K.P., J.S. Fuglestvedt, K. Hailemariam, and N. Stuber, 2005: Alternatives to the Global Warming Potential for Comparing Climate Impacts of Emissions of Greenhouse Gases. *Climatic Change*, **68**(3), 281–302, doi:[10.1007/s10584-005-1146-9](https://doi.org/10.1007/s10584-005-1146-9).
- Snider, G. et al., 2015: SPARTAN: a global network to evaluate and enhance satellite-based estimates of ground-level particulate matter for global health applications. *Atmospheric Measurement Techniques*, **8**(1), 505–521, doi:[10.5194/amt-8-505-2015](https://doi.org/10.5194/amt-8-505-2015).
- Solomon, P.A. et al., 2014: U.S. National PM2.5 Chemical Speciation Monitoring Networks – CSN and IMPROVE: Description of networks. *Journal of the Air & Waste Management Association*, **64**(12), 1410–1438, doi:[10.1080/10962247.2014.956904](https://doi.org/10.1080/10962247.2014.956904).
- Stevenson, D.S. et al., 2013: Tropospheric ozone changes, radiative forcing and attribution to emissions in the Atmospheric Chemistry and Climate Model Intercomparison Project (ACCMIP). *Atmospheric Chemistry and Physics*, **13**(6), 3063–3085, doi:[10.5194/acp-13-3063-2013](https://doi.org/10.5194/acp-13-3063-2013).
- Swart, N.C. et al., 2019: CCCma CanESM5 model output prepared for CMIP6 DAMIP ssp245-covid. Earth System Grid Federation, doi:[10.22033/esgf/cmip6.14913](https://doi.org/10.22033/esgf/cmip6.14913).
- Takemura, T., 2019a: MIROC MIROC6 model output prepared for CMIP6 AerChemMIP. Earth System Grid Federation, doi:[10.22033/esgf/cmip6.9121](https://doi.org/10.22033/esgf/cmip6.9121).
- Takemura, T., 2019b: MIROC MIROC6 model output prepared for CMIP6 AerChemMIP hist-piAer. Earth System Grid Federation, doi:[10.22033/esgf/cmip6.9123](https://doi.org/10.22033/esgf/cmip6.9123).
- Takemura, T., 2019c: MIROC MIROC6 model output prepared for CMIP6 AerChemMIP histSST. Earth System Grid Federation, doi:[10.22033/esgf/cmip6.9125](https://doi.org/10.22033/esgf/cmip6.9125).
- Takemura, T., 2019d: MIROC MIROC6 model output prepared for CMIP6 AerChemMIP histSST-piAer. Earth System Grid Federation, doi:[10.22033/esgf/cmip6.9127](https://doi.org/10.22033/esgf/cmip6.9127).
- Tang, Y. et al., 2019: MOHC UKESM1.0-LL model output prepared for CMIP6 CMIP historical. Earth System Grid Federation, doi:[10.22033/esgf/cmip6.6113](https://doi.org/10.22033/esgf/cmip6.6113).
- Thornhill, G.D. et al., 2021: Effective radiative forcing from emissions of reactive gases and aerosols – a multi-model comparison. *Atmospheric Chemistry and Physics*, **21**(2), 853–874, doi:[10.5194/acp-21-853-2021](https://doi.org/10.5194/acp-21-853-2021).
- Turner, A.J., C. Frankenberg, P.O. Wennberg, and D.J. Jacob, 2017: Ambiguity in the causes for decadal trends in atmospheric methane and hydroxyl. *Proceedings of the National Academy of Sciences*, **114**(21), 5367–5372, doi:[10.1073/pnas.1616020114](https://doi.org/10.1073/pnas.1616020114).
- Van Dingenen, R. et al., 2018: TM5-FASST: a global atmospheric source-receptor model for rapid impact analysis of emission changes on air quality and short-lived climate pollutants. *Atmospheric Chemistry and Physics*, **18**(21), 16173–16211, doi:[10.5194/acp-18-16173-2018](https://doi.org/10.5194/acp-18-16173-2018).
- van Marle, M.J.E. et al., 2017: Historic global biomass burning emissions for CMIP6 (BB4CMIP) based on merging satellite observations with proxies and fire models (1750–2015). *Geoscientific Model Development*, **10**(9), 3329–3357, doi:[10.5194/gmd-10-3329-2017](https://doi.org/10.5194/gmd-10-3329-2017).
- van Vuuren, D.P. et al., 2011: The representative concentration pathways: an overview. *Climatic Change*, **109**(1), 5, doi:[10.1007/s10584-011-0148-z](https://doi.org/10.1007/s10584-011-0148-z).
- Vandyck, T., K. Keramidas, S. Tchung-Ming, M. Weitzel, and R. Van Dingenen, 2020: Quantifying air quality co-benefits of climate policy across sectors and regions. *Climatic Change*, **163**(3), 1501–1517, doi:[10.1007/s10584-020-02685-7](https://doi.org/10.1007/s10584-020-02685-7).
- Wang, Y. et al., 2019: Trends in particulate matter and its chemical compositions in China from 2013–2017. *Science China Earth Sciences*, **62**(12), 1857–1871, doi:[10.1007/s11430-018-9373-1](https://doi.org/10.1007/s11430-018-9373-1).
- Weinstein, J.P., S.R. Hedges, and S. Kimbrough, 2010: Characterization and aerosol mass balance of PM2.5 and PM10 collected in Conakry, Guinea during the 2004 Harmattan period. *Chemosphere*, **78**(8), 980–988, doi:[10.1016/j.chemosphere.2009.12.022](https://doi.org/10.1016/j.chemosphere.2009.12.022).
- Yukimoto, S. et al., 2019a: MRI MRI-ESM2.0 model output prepared for CMIP6 AerChemMIP. Earth System Grid Federation, doi:[10.22033/esgf/cmip6.633](https://doi.org/10.22033/esgf/cmip6.633).
- Yukimoto, S. et al., 2019b: MRI MRI-ESM2.0 model output prepared for CMIP6 AerChemMIP histSST. Earth System Grid Federation, doi:[10.22033/esgf/cmip6.6835](https://doi.org/10.22033/esgf/cmip6.6835).
- Yukimoto, S. et al., 2019c: MRI MRI-ESM2.0 model output prepared for CMIP6 AerChemMIP ssp370-lowNTCF. Earth System Grid Federation, doi:[10.22033/esgf/cmip6.6917](https://doi.org/10.22033/esgf/cmip6.6917).
- Yukimoto, S. et al., 2019d: MRI MRI-ESM2.0 model output prepared for CMIP6 AerChemMIP ssp370SST. Earth System Grid Federation, doi:[10.22033/esgf/cmip6.6918](https://doi.org/10.22033/esgf/cmip6.6918).
- Yukimoto, S. et al., 2019e: MRI MRI-ESM2.0 model output prepared for CMIP6 CMIP historical. Earth System Grid Federation, doi:[10.22033/esgf/cmip6.6842](https://doi.org/10.22033/esgf/cmip6.6842).
- Yukimoto, S. et al., 2019f: MRI MRI-ESM2.0 model output prepared for CMIP6 DAMIP. Earth System Grid Federation, doi:[10.22033/esgf/cmip6.634](https://doi.org/10.22033/esgf/cmip6.634).
- Yukimoto, S. et al., 2019g: MRI MRI-ESM2.0 model output prepared for CMIP6 ScenarioMIP. Earth System Grid Federation, doi:[10.22033/esgf/cmip6.638](https://doi.org/10.22033/esgf/cmip6.638).
- Yukimoto, S. et al., 2019h: MRI MRI-ESM2.0 model output prepared for CMIP6 ScenarioMIP ssp126. Earth System Grid Federation, doi:[10.22033/esgf/cmip6.6909](https://doi.org/10.22033/esgf/cmip6.6909).
- Yukimoto, S. et al., 2019i: MRI MRI-ESM2.0 model output prepared for CMIP6 ScenarioMIP ssp245. Earth System Grid Federation, doi:[10.22033/esgf/cmip6.6910](https://doi.org/10.22033/esgf/cmip6.6910).
- Yukimoto, S. et al., 2019j: MRI MRI-ESM2.0 model output prepared for CMIP6 ScenarioMIP ssp370. Earth System Grid Federation, doi:[10.22033/esgf/cmip6.6915](https://doi.org/10.22033/esgf/cmip6.6915).
- Yukimoto, S. et al., 2019k: MRI MRI-ESM2.0 model output prepared for CMIP6 ScenarioMIP ssp585. Earth System Grid Federation, doi:[10.22033/esgf/cmip6.6929](https://doi.org/10.22033/esgf/cmip6.6929).
- Yukimoto, S. et al., 2020a: MRI MRI-ESM2.0 model output prepared for CMIP6 AerChemMIP hist-piAer. Earth System Grid Federation, doi:[10.22033/esgf/cmip6.6826](https://doi.org/10.22033/esgf/cmip6.6826).
- Yukimoto, S. et al., 2020b: MRI MRI-ESM2.0 model output prepared for CMIP6 AerChemMIP histSST-piAer. Earth System Grid Federation, doi:[10.22033/esgf/cmip6.6837](https://doi.org/10.22033/esgf/cmip6.6837).
- Yukimoto, S. et al., 2020c: MRI MRI-ESM2.0 model output prepared for CMIP6 AerChemMIP ssp370-lowNTCFCH4. Earth System Grid Federation, doi:[10.22033/esgf/cmip6.13529](https://doi.org/10.22033/esgf/cmip6.13529).
- Yukimoto, S. et al., 2020d: MRI MRI-ESM2.0 model output prepared for CMIP6 AerChemMIP ssp370pdSST. Earth System Grid Federation, doi:[10.22033/esgf/cmip6.11409](https://doi.org/10.22033/esgf/cmip6.11409).
- Zhang, F. et al., 2012: Chemical compositions and extinction coefficients of PM2.5 in peri-urban of Xiamen, China, during June 2009–May 2010. *Atmospheric Research*, **106**, 150–158, doi:[10.1016/j.atmosres.2011.12.005](https://doi.org/10.1016/j.atmosres.2011.12.005).
- Zhao, P.S. et al., 2013: Characteristics of concentrations and chemical compositions for PM2.5 in the region of Beijing, Tianjin, and Hebei, China. *Atmospheric Chemistry and Physics*, **13**(9), 4631–4644, doi:[10.5194/acp-13-4631-2013](https://doi.org/10.5194/acp-13-4631-2013).
- Ziehn, T. et al., 2020: CSIRO ACCESS-ESM1.5 model output prepared for CMIP6 DAMIP ssp245-covid. Earth System Grid Federation, doi:[10.22033/esgf/cmip6.14937](https://doi.org/10.22033/esgf/cmip6.14937).

